Global Biogeochemical Cycles

RESEARCH ARTICLE
10.1029/2022GB007610

Decoupling of Barium and Silicon at the Congo River-Dominated Southeast Atlantic Margin: Insights From Combined Barium and Silicon Isotopes

Zhouling Zhang[1], Yang Yu[1], Ed C. Hathorne[1], Lucia H. Vieira[1], Patricia Grasse[1,2], Christopher Siebert[1], Peer Rahlf[1], and Martin Frank[1]

[1]GEOMAR Helmholtz Centre for Ocean Research Kiel, Kiel, Germany, [2]German Centre for Integrative Biodiversity Research (iDiv) Halle-Jena-Leipzig, Leipzig, Germany

Key Points:

- Stronger enrichment of dissolved barium (dBa) than silicon (dSi) observed in the shelf-zone of the Congo plume
- Diatom silica production has negligible effect on dissolved Ba isotopic compositions in large river plumes
- Strong dBa enrichment (up to 24 nM) in the deep water of the northern Angola Basin likely originates from high benthic inputs

Supporting Information:

Supporting Information may be found in the online version of this article.

Correspondence to:

Z. Zhang,
zzhang@geomar.de

Citation:

Zhang, Z., Yu, Y., Hathorne, E. C., Vieira, L. H., Grasse, P., Siebert, C., et al. (2023). Decoupling of barium and silicon at the Congo River-dominated Southeast Atlantic margin: Insights from combined barium and silicon isotopes. *Global Biogeochemical Cycles*, *37*, e2022GB007610. https://doi.org/10.1029/2022GB007610

Received 14 OCT 2022
Accepted 22 APR 2023

Author Contributions:

Conceptualization: Zhouling Zhang, Ed C. Hathorne, Martin Frank
Formal analysis: Zhouling Zhang, Yang Yu, Lucia H. Vieira
Supervision: Martin Frank
Visualization: Zhouling Zhang
Writing – original draft: Zhouling Zhang

Abstract The correlation between concentrations of dissolved barium (dBa) and silicon (dSi) in the modern ocean supports the use of Ba as a paleoceanographic proxy. However, the mechanisms behind their linkage and the exact processes controlling oceanic Ba cycling remain enigmatic. To discern the extent to which this association arises from biogeochemical processes versus physical mixing, we examine the behavior of Ba and Si at the Congo River-dominated Southeast Atlantic margin where active biological processes and large boundary inputs override the large-scale ocean circulation. Here we present the first combined measurements of dissolved stable Ba (δ^{138}Ba) and Si (δ^{30}Si) isotopes as well as Ba and Si fluxes estimated based on ^{228}Ra from the Congo River mouth to the northern Angola Basin. In the surface waters, river-borne particle desorption or dissolution and shelf inputs lead to non-conservative additions of both dBa and dSi to the Congo-shelf-zone, with the Ba flux increasing more strongly than that of Si across the shelf. In the epipelagic and mesopelagic layers, Ba and Si are decoupled likely due to different depths of in situ barite precipitation and biogenic silica production. In the deep waters of the northern Angola Basin, we observe large enrichment of dBa, likely originating from high benthic inputs from the Congo deep-sea fan sediments. Our results reveal different mechanisms controlling the biogeochemical cycling of Ba and Si and highlight a strong margin influence on marine Ba cycling. Their close association across the global ocean must therefore mainly be a consequence of the large-scale ocean circulation.

Plain Language Summary Across the oceans from surface waters to the deep, dissolved barium (Ba) and silicon (Si) concentrations are strongly correlated. However, we still do not fully understand the mechanisms behind this pattern. Rivers and continental shelves are the major sources of both Ba and Si to seawater and here we study the release and cycling of Ba and Si at the Congo River-dominated central west African margin. By measuring the stable isotopes of both Ba and Si in the same seawater samples, and estimating the elemental fluxes of Ba and Si along the Congo River plume based on radioactive radium isotopes, we find differing behavior of Ba and Si in the surface Congo plume and the subsurface and deep waters of the adjacent northern Angola Basin. These different behaviors result from contrasting carriers of Ba and Si to the coastal ocean, as well as fundamentally different biological and chemical processes controlling the cycling of Ba and Si in the coastal water and sediments. The close association of dissolved Si and Ba across the global ocean must therefore mainly result from the large-scale ocean circulation.

1. Introduction

Barium (Ba) is an important tracer of ocean circulation (Le Roy et al., 2018), freshwater inputs (Guay et al., 2009) as well as export production (Jeandel et al., 2000) in the modern ocean. Ba-based proxies have therefore been used for reconstructions of past ocean conditions, including productivity (e.g., Dymond et al., 1992), alkalinity (e.g., Lea, 1993), and river runoff (e.g., Gebregiorgis et al., 2016; Weldeab et al., 2007). However, the reliable use of Ba-based proxies is still hampered by gaps in our knowledge regarding processes that regulate the distribution of Ba in different ocean settings (Jeandel et al., 1996; McManus et al., 1998). The pelagic Ba distribution is primarily driven by organic matter-associated removal in the euphotic zone, barite precipitation in particle-associated microenvironments during microbial oxidation of organic matter in the mesopelagic zone, and barite dissolution in deep waters (Cao et al., 2020; Chow & Goldberg, 1960; Dehairs et al., 1980; Horner & Crockford, 2021; Martinez-Ruiz et al., 2019).

Writing – review & editing: Zhouling Zhang, Yang Yu, Ed C. Hathorne, Lucia H. Vieira, Patricia Grasse, Christopher Siebert, Peer Rahlf, Martin Frank

The concentrations of dissolved Ba (dBa) in the open ocean are closely correlated with those of dissolved silicic acid ($Si(OH)_4$, hereafter referred to as dSi) (Bacon & Edmond, 1972; Chan et al., 1977; Jeandel et al., 1996). Si distribution is controlled by the biological uptake of various silicifiers, in particular diatoms, and the subsequent dissolution of biogenic silica (bSi) within and below the euphotic zone (Tréguer et al., 2021). It has been suggested that organic and skeletal debris represent a significant proportion of the total particulate Ba in surface waters (Carter et al., 2020; Dehairs et al., 1980; Martinez-Ruiz et al., 2019). However, several laboratory experiments have revealed negligible intracellular uptake of Ba by diatoms (Fisher et al., 1991; Sternberg et al., 2005). Alternatively, it has been argued that similarities between dBa and dSi profiles and their linear correlation in global seawater are the result of common hydrodynamic controls resulting in the basin-scale distributions of dBa and dSi mainly modulated by ocean circulation (Bacon & Edmond, 1972; Bates et al., 2017; Chan et al., 1977; Hsieh & Henderson, 2017). The exact mechanism leading to the observed Ba-Si correlation remains ambiguous for two reasons: (a) the correlation between dBa and dSi is significantly closer than that of dBa and other major nutrients such as nitrate and phosphate, which are required by phytoplankton; (b) unlike dSi, dBa is not an essential nutrient for phytoplankton growth (Chan et al., 1977; Jacquet et al., 2005; Jeandel et al., 1996). It remains unconstrained whether bSi is a significant particulate Ba carrier in surface water (Cao et al., 2020; Sternberg et al., 2005), and the extent to which this pattern arises from non-conservative biogeochemical processes versus water mass mixing (Horner et al., 2021). Furthermore, it has frequently been observed that the correlation between Ba and Si deviates near ocean margins or in basins with limited circulation (Chan et al., 1977; Rahman et al., 2022). Therefore, a more complete mechanistic understanding of the linkages (or the lack thereof) between Ba and Si in such oceanic settings is needed to understand the oceanographic processes that control the oceanic Ba cycle and to allow more reliable use of Ba-based proxies archived in marine sediments for the reconstruction of past oceanic environments.

This study thus aims to investigate the relationship between dBa and dSi at a river-dominated ocean margin where local processes and boundary inputs largely override the dominant control of ocean circulation and allow further insight into the controlling factors of Ba and Si biogeochemistry. In particular, it has been shown recently that land-sea interactions play a major role in the ocean budget of both elements (Rahman et al., 2022; Tréguer et al., 2021). In estuarine systems, salinity-induced desorption of Ba from the riverine particle load leads to a dBa maximum at low-mid salinity (Coffey et al., 1997; Edmond et al., 1978), while productivity-related depletion of Ba has also been observed in surface waters (Joung & Shiller, 2014; Nozaki et al., 2001). The highly dynamic interaction between sediments and seawater along continental margins also affects the biogeochemical cycle of Ba significantly. For example, the removal of dBa due to the resuspension of oxyhydroxides can occur along continental slopes (Coffey et al., 1997; Dymond & Collier, 1996), whereas reductive dissolution of manganese (Mn) (hydr)oxides in low oxygen estuarine/shelf sediments or subterranean estuaries can lead to the release of Ba (Charette & Sholkovitz, 2006; Hong et al., 2018). In addition, submarine groundwater discharge (SGD) can contribute large amounts of dBa to the marginal system (Mayfield et al., 2021; Moore, 1997; Rahman et al., 2022). dSi, on the other hand, is predominantly controlled by (diatom) productivity (DeMaster et al., 1996), dissolution of amorphous silica (biogenic and lithogenic material (Frings et al., 2016; Tréguer et al., 2021)), and SGD admixture (Cho et al., 2018; Rahman et al., 2019).

Recently, the stable isotopic composition of Ba ($\delta^{138}Ba$) has been developed to investigate the variability of key aspects of marine Ba biogeochemistry, given that in the upper ocean light Ba isotopes are either preferentially incorporated during the precipitation of barite (Bridgestock et al., 2018; Cao et al., 2016; Horner et al., 2015, 2017; Yu et al., 2022) or preferentially adsorbed onto particles (Cao et al., 2020). Similarly, over the past two decades, the stable isotopic composition of Si ($\delta^{30}Si$) has been used as a tool to identify Si sources and to track Si biogeochemical cycling and Si utilization on various temporal and spatial scales given that silicifiers preferentially incorporate the lighter Si isotopes to build their silica skeletons or shells (cf., De La Rocha et al., 1997; Sutton et al., 2018). In general, $\delta^{138}Ba$ and $\delta^{30}Si$ display similar distributions in the ocean. Major rivers are characterized by relatively light isotopic signatures of both Ba (average ~0.2‰) and Si (average ~1.3‰), reflecting the dissolution of lithogenic materials, whereas surface seawater shows significantly heavier isotopic signatures of both Ba (0.3–0.6‰) and Si (up to 3–4‰) due to the preferential removal of the light isotopes via the processes described above (Bridgestock et al., 2021; Cao et al., 2021; Frings et al., 2016; Hsieh & Henderson, 2017; Sutton et al., 2018; Yu et al., 2022; Zhang, Cao, et al., 2020). Deep seawaters are typically enriched in isotopically light Si and Ba compared to the surface seawaters as a result of remineralization processes and water mass mixing (Bates et al., 2017; De Souza, Reynolds, Johnson, et al., 2012; De Souza,

Reynolds, Rickli, et al., 2012; Horner et al., 2015). Apart from biogeochemical processes, both isotopic systems also provide insights into their various sources and sinks in marginal regions (Whitmore et al., 2022; Zhang, Sun, et al., 2020). As such, the combined use of δ^{138}Ba and δ^{30}Si is proposed to provide new insights into the linkages between Ba and Si cycling.

To elucidate the interplay of local and regional boundary inputs and large-scale ocean circulation affecting the biogeochemical cycling of Ba and Si, we investigated the relationship between Ba and Si at one of the largest major river-dominated ocean margins, the Congo-influenced West African margin. The Congo River is the second-largest river on Earth in terms of freshwater discharge and the twelfth largest for annual total suspended sediment load (Hopkins et al., 2013). The Congo River estuary is characterized by a deep canyon that connects the river to the deep ocean by cutting through the continental shelf, which impacts the plume and shelf dynamics as well as estuarine circulation (Savoye et al., 2009). Due to the presence of the deep canyon, river water rapidly flows into the ocean as a thin layer of freshwater with nearly horizontal isohalines (Cadée, 1978). Its river plume delivers high fluxes of dissolved trace elements (TEs) (Menzel Barraqueta, 2018; Vieira et al., 2020) and rare earth elements (REEs) (Rahlf et al., 2021) to the oligotrophic Southeast Atlantic Ocean. In addition, large contributions of TEs and REEs released from river-borne particles or shelf sediments were found (Rahlf et al., 2021; Vieira et al., 2020). Additionally, the large active Congo canyon funnels a large amount of the riverine sediment load to the abyssal Atlantic Ocean bypassing the shelf via turbidity currents (Rabouille et al., 2019; Talling et al., 2022). The Congo Deep-Sea Fan extends over 1,000 km from the Congo-Angola coast with a surface area of 300,000 km^2 and is one of the largest submarine fan systems in the world (Savoye et al., 2009). In this study, we combine the distributions of δ^{138}Ba and δ^{30}Si, as well as Ba and Si fluxes estimated based on radioactive radium isotopes (^{228}Ra) to evaluate the biogeochemical cycles of Ba and Si and their relationship during transport from the Congo River mouth along the southwestern African shelf to the open northern Angola Basin, as part of the GEOTRACES eastern South Atlantic Ocean GA08 cruise.

2. Methods

2.1. Sampling

Seawater samples were collected during GEOTRACES cruise GA08 with German RV Meteor (M121) in November and December 2015 (beginning of austral summer). The cruise track followed the north-westerly flow path of the plume from the Congo mouth and shelf zone (defined as the shelf region where Congo waters first encounter the Atlantic Ocean) to the latitudinal off-shelf section at 3°S in the northern Angola Basin (Figure 1). The contribution of other rivers to the low salinity plume observed in the study region is considered minimal (Vieira et al., 2020). The cruise track covered the Southwestern African shelf area to determine the amount and lateral extent of elemental inputs from the Congo River. Surface water samples were sampled under trace metal clean conditions using a towed fish while the vessel was steaming, which allowed continuous clean pumping directly into the clean laboratory container. For subsurface/deep waters, contaminant-prone trace metals, for example, Fe, Mn, Cu, and Zn, were sampled using the GEOMAR trace metal clean CTD rosette equipped with trace metal clean Go-Flo bottles. The samples were then filtered in the trace metal clean sampling lab onboard (Vieira et al., 2020). Less contaminant-prone elements such as Si, Ba, Nd, and Hf were collected using a stainless steel CTD rosette equipped with Niskin bottles. On board, samples for Si and Ba measurements were filtered through a nitrocellulose acetate filter (0.45 μm pore diameter) using a peristaltic pump and were then acidified with concentrated distilled HCl (pH ∼ 2) and stored in 2 L acid-cleaned PE bottles. Unfortunately, it was not possible to collect samples in the low-mid salinity zone (salinity 0–20) because of commercial hydrocarbon extraction activities on the shelf, but Congo River freshwater samples were taken upstream by boat in May, July, and October 2017 near the center of the river (∼6°S, 12.5°E; stations 12.1–12.3) (Rahlf et al., 2021). Sampling covered the low discharge period in summer (July), the peak discharge in autumn/winter (October), and the intermediate discharge in May (Materia et al., 2012). The samples were collected in 10 L acid-cleaned plastic bottles, filtered through AcroPak™500 cartridges (Supor; 0.2 μm) within 2 hr after collection, and then acidified with concentrated distilled HCl (pH ∼2). In the home laboratory at GEOMAR, 100 mL aliquots of each sample were transferred into acid-cleaned LDPE bottles for isotopic measurements. Sampling blanks derived by filtration of MQ water on board under the same conditions as the samples (nitrocellulose acetate filter or AcroPak™500 cartridges) are all in the pmol/kg range and negligible compared to sample concentrations. The hydrological settings of the Congo River plume and the Angola Basin are described in Text S1 of Supporting Information S1.

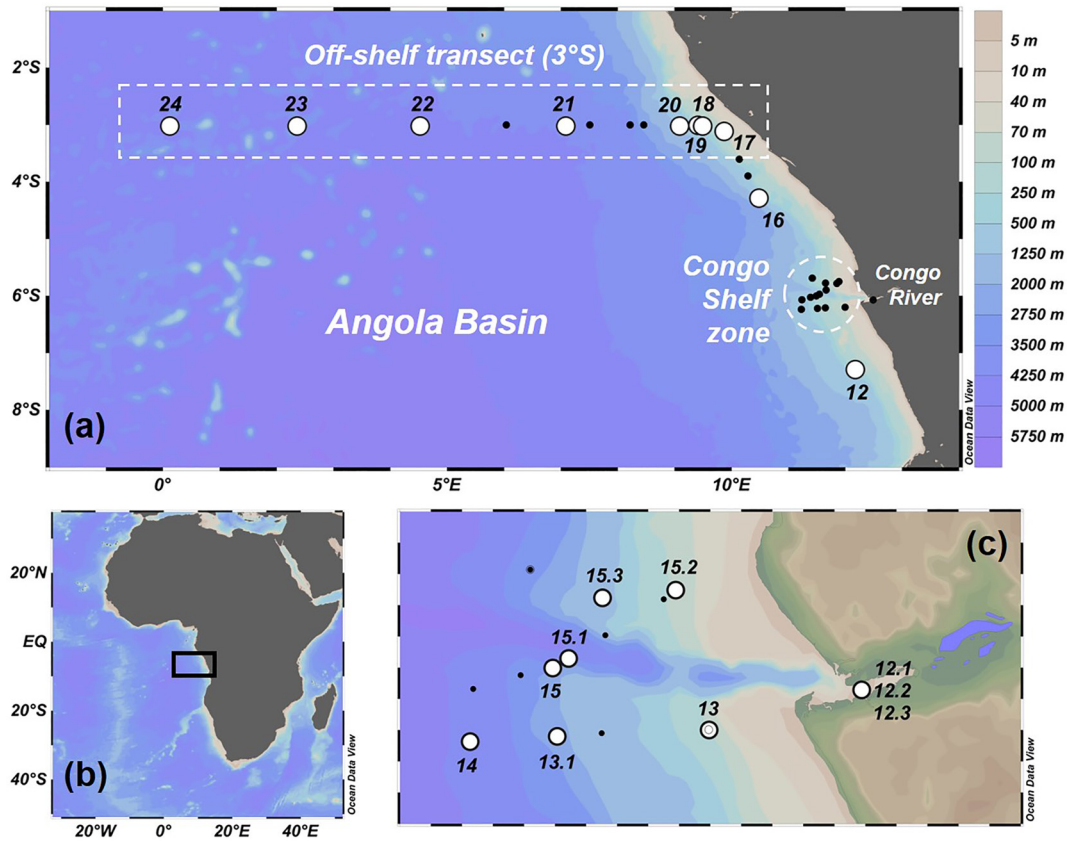

Figure 1. (a) Map showing sampling stations occupied during cruise M121 following the Congo River plume along its flow path off the West African coast to a connected off-shelf latitudinal section at 3°S in the northern Angola Basin. White circles denote stations with full water column sampling, while back dots denote additional FISH stations. (b) Zoom out map showing the location of the study site. (c) Zoom in map showing sampling stations in the Congo River and Congo-shelf-zone. Stations 12.1, 12.2, and 12.3 represent the sampling locations of Congo River freshwater endmember samples taken in May, July, and October 2017, respectively. Figure produced using Ocean Data View (Schlitzer, 2021).

2.2. Analytical Methods of Ba and Si Isotope Measurement

The dBa concentrations were analyzed by isotope dilution using an Agilent 7500ce inductively coupled plasma mass spectrometer at GEOMAR, Kiel with a precision of ±2% (2 standard deviations, 2SD of repeated sample measurements). Ba isotopic compositions were measured using a double spike (^{130}Ba-^{135}Ba) technique and are reported in ‰ deviations from the international Ba standard NIST SRM 3104a ($Ba(NO_3)_2$, Lot: 070222; $\delta^{138}Ba = [(^{138}Ba/^{134}Ba)_{sample}/(^{138}Ba/^{134}Ba)_{standard} - 1] \times 1{,}000$) (Cao et al., 2016; Horner et al., 2015). Separation of Ba from the sample matrix was achieved by a method modified from Horner et al. (2015) and described in detail by Yu et al. (2020). Briefly, spiked samples were co-precipitated with $CaCO_3$ using a pre-treated Ba-free Na_2CO_3 solution and purified twice by cation-exchange chromatography (BIORAD® AG50W-X8 resin, 200–400 μm mesh-size, 1.4 mL resin bed) with an average yield of 90% for the entire chemical preparation procedure. Stable Ba isotope measurements were performed using a Thermo Fisher Neptune Plus® MC-ICP-MS at GEOMAR, Kiel. Each sample solution was analyzed three to four times in a single measurement session, resulting in a δ^{138}Ba sample reproducibility between ±0.01 and ±0.06‰ (2SD). Most samples were analyzed repeatedly, including co-precipitation and column chemistry. Long-term repeated measurements of in-house seawater reference materials yielded δ^{138}Ba values of 0.55 ± 0.05‰ (2SD, $N = 26$) and 0.47 ± 0.04‰ (2SD, $N = 18$) for BATS 15 and 2,000 m, respectively, over a course of three years. International seawater reference samples SAFe surface and SAFe 1,000 m yielded values of 0.62 ± 0.03‰ (2SD, $N = 6$) and 0.29 ± 0.03‰ (2SD, $N = 19$), respectively, within error identical to those published in Cao et al. (2021), Geyman et al. (2019), and Hsieh & Henderson (2017). Carbonate reference material JCp-1 yielded a value of 0.29 ± 0.03‰ (2SD, $N = 27$), which is also identical within error to those reported (see references above). Errors reported in the text below are the 2SD of repeated sample measurements.

The dSi concentrations were analyzed onboard Meteor by segmented flow injection analysis using a QUAATRO (Seal Analytical) auto-analyzer. Si isotopic compositions were measured using a NuPlasma HR MC-ICP-MS (Nu Instruments™) at GEOMAR, Kiel, and are reported in ‰ deviations from the international Si standard NBS28 ($\delta^{30}Si = [(^{30}Si/^{28}Si)_{sample}/(^{30}Si/^{28}Si)_{standard}-1] \times 1{,}000$). Si in all samples was pre-concentrated and separated from the major matrix elements using a two-step Magnesium Co-Precipitation (MAGIC) technique (Reynolds et al., 2006), and was further purified using cation-exchange chromatography (Georg et al., 2006). Low-salinity samples were pre-treated with Mg^{2+} addition (Zhang, Cao, et al., 2020; Zhang, Sun, et al., 2020). Each purified sample solution was analyzed three to four times in a single measurement session using a standard-sample bracketing technique. The analysis of individual samples was repeated two to six times in different analytical sessions. Most of the measurements were repeated in full, including the MAGIC co-precipitation and column chemistry. Sample reproducibility (2SD) generally ranged from 0.05 to 0.24‰. Repeated measurements of the international reference materials diatomite, IRMM-018, ALOHA 300 m, and ALOHA 1,000 m during the course of sample analyses gave average $\delta^{30}Si$ values of 1.22 ± 0.16‰ (2SD, $N = 23$), -1.45 ± 0.13‰ (2SD, $N = 5$), 1.72 ± 0.15‰ (2SD, $N = 12$), and 1.23 ± 0.18‰ (2SD, $N = 27$), which are in good agreement with those obtained during inter-laboratory comparisons (Grasse et al., 2017; Reynolds et al., 2007). Errors reported in the text below are the 2SD of repeated sample measurements. More details of Ba and Si isotope analyses can be found in Text S2 and Figure S1 of Supporting Information S1.

2.3. Ba and Si Flux Estimations

To investigate estuarine Ba and Si behavior and assess the Congo's impact on the budgets of these elements in the South Atlantic Ocean, we determined their fluxes from the Congo River to the proximal shelf (hereafter the Congo-shelf-zone) and further to the distal plume section at the off-shelf 3°S transect. Ba and Si fluxes from the Congo River were estimated by multiplying the average riverine dBa and dSi concentrations at the river mouth by the river discharge (1.3×10^{12} m^3/yr; Milliman & Farnsworth, 2011). Ba and Si fluxes into the Congo-shelf zone and off-shelf fluxes along the 3°S transect were determined based on radium isotope (^{228}Ra) distributions following the approach in Vieira et al. (2020), which was also applied by Rahlf et al. (2021) to calculate Nd and Hf fluxes based on samples taken during the same cruise.

Briefly, ^{228}Ra flux ($3.4 \pm 0.9 \times 10^{21}$ atoms/yr) into the Congo-shelf zone was determined by dividing the ^{228}Ra inventory by the residence time of the waters in this region (Vieira et al., 2020). Ba flux was determined by multiplying the ^{228}Ra flux with the averaged ratio between dBa concentrations (in samples with the lowest measured salinity (i.e., <29 PSU)) and the ^{228}Ra Congo-shelf-endmember ($dBa/^{228}Ra = 1.64 \pm 0.51 \times 10^{-4}$ nmol/atom). The Si flux was estimated using the same approach ($dSi/^{228}Ra = 1.05 \pm 0.38 \times 10^{-1}$ nmol/atom). This approach includes all the ^{228}Ra, Ba and Si dissolved forms derived from the dissolved phase and the release from particulate phases (i.e., desorption from river-borne particles and shelf sediments near the river mouth).

^{228}Ra as a geochemical tracer can aid in tracking the horizontal dispersion of river-plume-derived Ba and Si; the net Ba and Si fluxes from the Congo plume can be linearly scaled with the ^{228}Ra flux within the extension of the diffusion-dominant system (see Vieira et al., 2020). Thus, the Ba off-shelf flux along the 3°S transect was determined using the ^{228}Ra flux as the same approach applied to the Congo-shelf-zone. The off-shelf ^{228}Ra flux of $6.2 \pm 2.0 \times 10^{21}$ (atoms/yr) was multiplied by the $\Delta dBa/\Delta Ra$ ratio, where ΔdBa and ΔRa are the difference between the dBa and Ra shelf-endmembers (dBa_{shelf} and Ra_{shelf}) and their off-shelf endmembers ($dBa_{offshelf}$ and $Ra_{offshelf}$), for example, $Ba\text{-flux} = Ra\text{-flux} \times [(dBa_{shelf} - dBa_{offshelf})/(Ra_{shelf} - Ra_{offshelf})]$. The dBa and Ra shelf-endmembers are the average concentrations of the dBa and ^{228}Ra in surface waters (3–4 m water depth) over the shelf (stations 17, 18, and 19), respectively. The off-shelf endmembers are the concentrations of dBa and ^{228}Ra at station 21. This approach is only valid in a diffusion-dominated system (Charette et al., 2016), as confirmed by the linear gradient in ^{228}Ra distributions between stations 17 and 21 (Vieira et al., 2020). The off-shelf Si flux was estimated using the same approach.

2.4. Ba* Calculation

As a measure of the decoupling of Ba and Si distributions, we use Ba*, defined as the deviation of dBa from the dBa-dSi correlation in a defined oceanic area (Bates et al., 2017; Horner et al., 2015). Deviations in Ba* could relate to the non-conservative behavior of either Ba or Si. In order to make our study region comparable in a

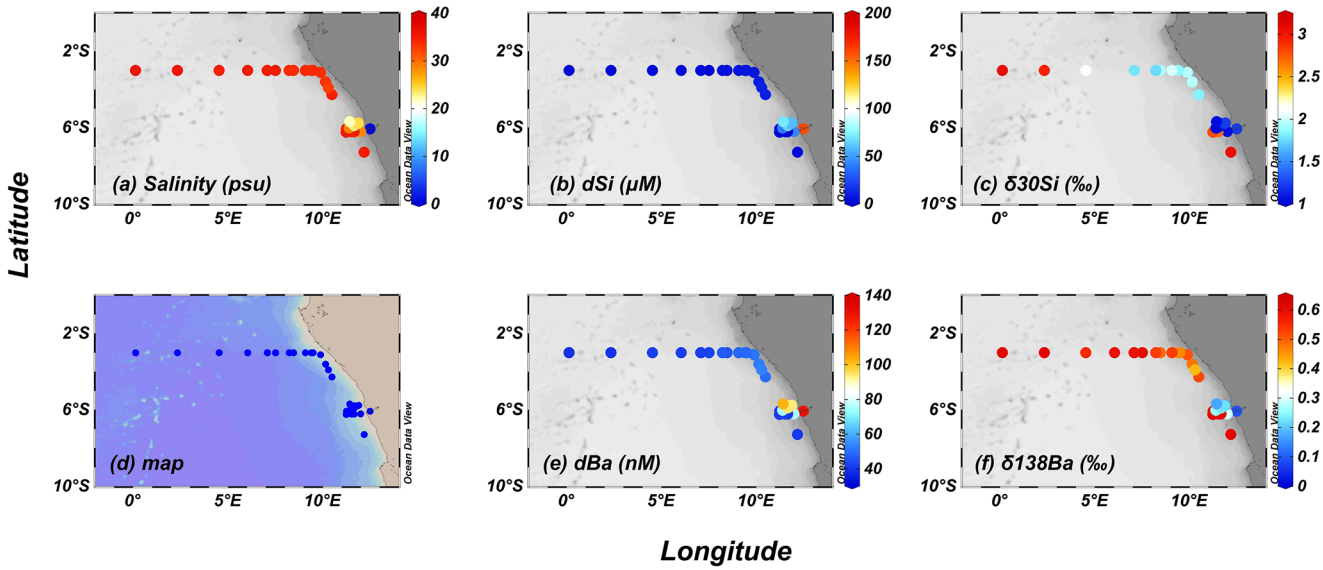

Figure 2. Surface distributions of (a) salinity, (b) dSi, (c) δ^{30}Si, (e) dBa, and (f) δ^{138}Ba. Panel (d) shows the sampling stations.

global context, we adopted the equation of Bates et al. (2017) to calculate Ba* based on York Regression of 1505 globally distributed dBa-dSi from the GEOSECS expeditions:

$$Ba^* = dBa - 0.63\,(\pm 0.002) \times dSi + 38.6\,(\pm 0.1)$$

Ba*, dBa, and dSi have units of nM, nM, and μM respectively.

In addition, in order to eliminate the potential influence of using different dBa-dSi correlations on our discussion, we also calculated Ba* based on a South Atlantic dBa-dSi correlation (Horner et al., 2015):

$$Ba^* = dBa - 0.52\,(\pm 0.01) \times dSi + 43.9\,(\pm 0.2)$$

as well as based on the regional dBa-dSi correlation in our study area (Figure S2 in Supporting Information S1; $dBa = 0.59 \times dSi + 42.7$, $R^2 = 0.91$):

$$Ba^* = dBa - 0.59\,(\pm 0.03) \times dSi + 42.7\,(\pm 1.4)$$

The choice of equation does not influence the resulting general Ba* pattern (see Section 3.2). Horner et al. (2015) also pointed out that even though different water masses are likely characterized by different preformed Ba* values, the depth profiles of Ba* are best interpreted in terms of deviations from invariant behavior. In brief, a positive Ba* value indicates dBa addition or increased dSi utilization relative to the mean regional or global trend, and vice versa.

3. Results and Discussion

3.1. Decoupling of Ba and Si in the Congo Surface Water Plume

3.1.1. Non-Conservative Addition of Ba in the Congo-Shelf-Zone

Surface water dBa distributions in the Congo estuary (Figures 2 and 3; Figure S3 in Supporting Information S1) are similar to other large river estuaries with decreasing concentrations from the river mouth to the open ocean (Bridgestock et al., 2021; Cao et al., 2021; Coffey et al., 1997). During estuarine mixing, surface water dBa and salinity show a significant negative linear relationship at salinities above 20 ($R^2 = 0.99$; Figure 3a),

$$dBa = 203.6\,(\pm 2.9) - 4.6\,(\pm 0.1) \times \text{salinity}$$

demonstrating conservative mixing in this salinity range. The effective river endmember dBa (dBa_{eff}) value of 203.6 ± 2.9 nM is obtained by extrapolation of the dBa-salinity linear regression to zero salinity and is 57%

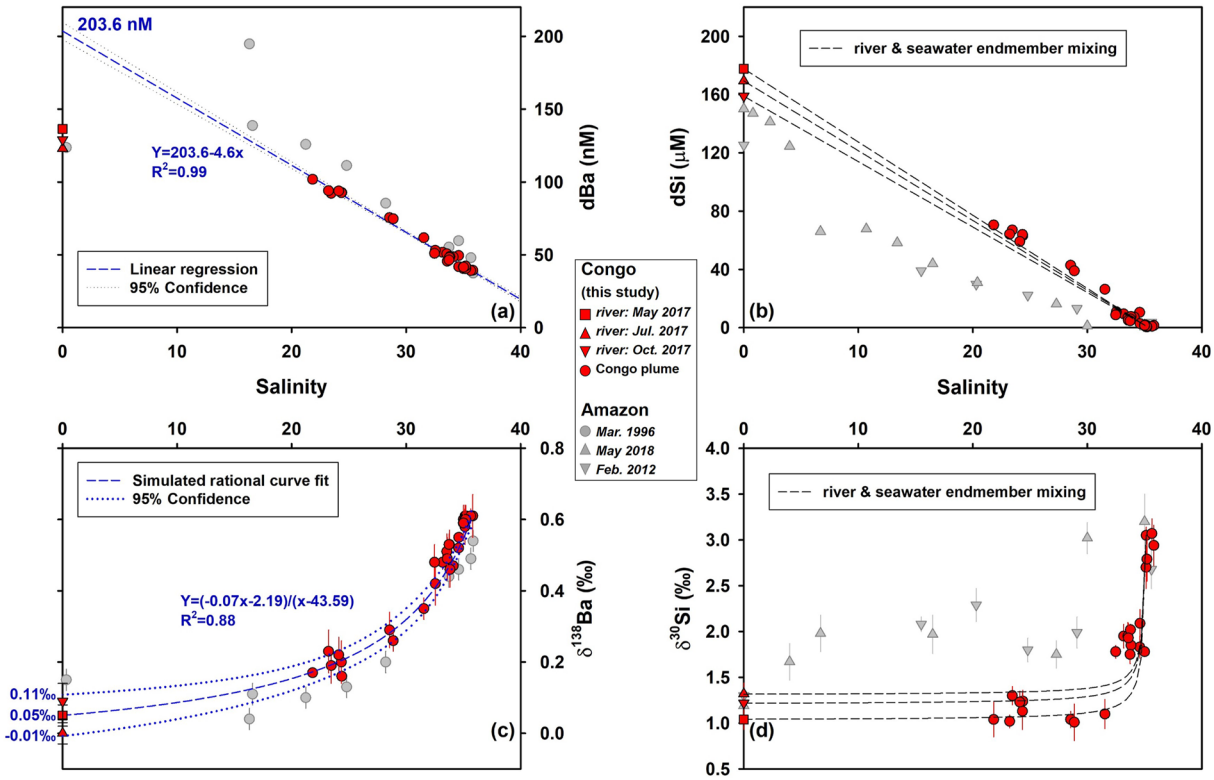

Figure 3. The distribution of (a) dBa, (b) dSi, (c) δ^{138}Ba, and (d) δ^{30}Si along salinity gradients in the Congo plume (this study; red symbols) and the Amazon plume (gray symbols). dBa and δ^{138}Ba data in the Amazon plume were obtained from Bridgestock et al. (2021), while dSi and δ^{30}Si data in the Amazon plume were obtained from Zhang, Cao, et al. (2020). Congo River values are shown in the red square (May 2017), upward triangle (July 2017), and downward triangle (October 2017). In panel (a), the blue dashed line represents the linear regression of dBa and salinity in the high-salinity zone, resulting in an effective-zero-salinity-endmember dBa (dBa_{eff}) concentration of 203.6 nM. In panel (c), the blue dashed line shows the rational regression of δ^{138}Ba signatures on salinity, resulting in an effective-zero-salinity-endmember δ^{138}Ba value of ~0.05‰ at a dBa_{eff} of 220.9 nM. The blue dotted lines represent the 95% confidence interval of the regression. In the right panels, the black dashed lines predict the conservative mixing for dSi (b) and δ^{30}Si (d) between the three river water endmembers and the seawater endmember.

higher than the measured dBa_{river} value (129.4 ± 6.7 nM). This reflects the magnitude of Ba addition in the low-mid salinity zone (Bridgestock et al., 2021; Cao et al., 2021; Coffey et al., 1997). Our estimate of dBa_{eff} is higher than a previous estimation (170 nmol/kg; Edmond et al., 1978), despite similar dBa_{river} values (~130 nM). This suggests a somewhat greater addition of Ba during our sampling period compared to the previous sampling campaign in November 1976, which may have been caused by seasonal variability of the environmental conditions in the estuary and/or the catchment. Surface waters at salinities above 20 are also characterized by a linear relationship between δ^{138}Ba values and inverse dBa concentrations ($R^2 = 0.98$, Figure 4a),

$$\delta^{138}\mathrm{Ba} = 28.97\,(\pm 0.83) \times \left(\frac{1}{\mathrm{dBa}}\right) - 0.11\,(\pm 0.02)$$

indicating conservative mixing with respect to δ^{138}Ba. The regression slope of 28.97 for the surface waters is significantly larger than that of the Atlantic data set ($K = 19.98$), summarized from the previously published datasets in the Atlantic Ocean and the Atlantic sector of the Southern Ocean (Bates et al., 2017; Bridgestock et al., 2018; Horner et al., 2015; Hsieh & Henderson, 2017). Riverine input of Ba with a light δ^{138}Ba signature shifts δ^{138}Ba in the surface water of our study area toward lower values below the Atlantic data array.

Based on Ra isotopes (method Section 2.3), Ba fluxes from the Congo River, to the Congo-shelf-zone, and the distal plume fluxes of the off-shelf transect at 3°S are calculated (Table 1, Figure 5). The Ba flux to the Congo-shelf-zone (76.09 ± 31.71 Gg/yr) is more than three times higher than that from the Congo River (23.11 ± 1.20 Gg/yr), pointing to 53 ± 32 Gg/yr of additional Ba input into the shelf zone (Table 1). The release of exchangeable Ba from riverine suspended particles due to exchange with major cations in seawater is considered the major source of Ba addition in most estuaries (Bridgestock et al., 2021; Coffey et al., 1997;

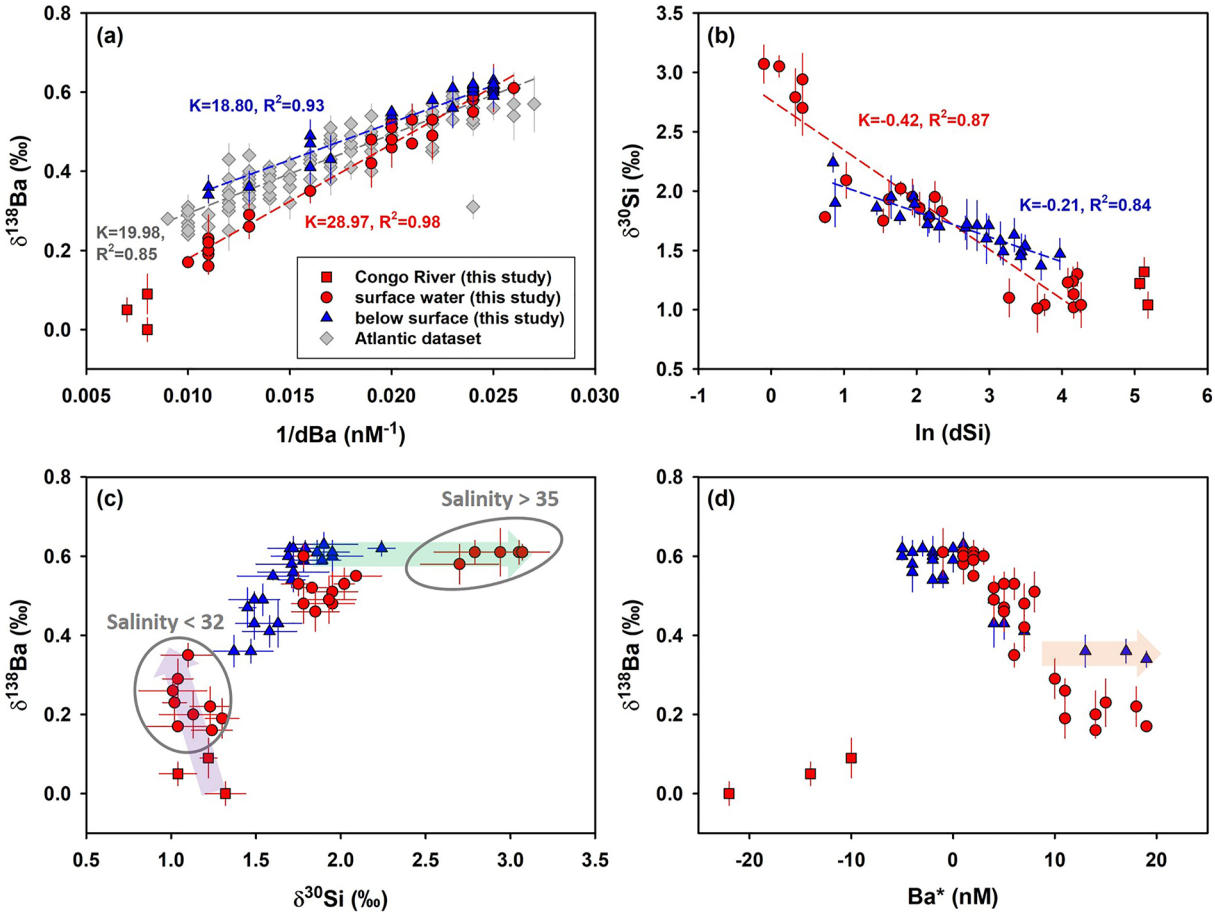

Figure 4. (a) δ^{138}Ba versus 1/dBa, (b) δ^{30}Si versus ln(dSi), (c) δ^{138}Ba versus δ^{30}Si, and (d) δ^{138}Ba versus Ba*. The Ba* values are calculated using the global dBa-dSi correlation in Bates et al. (2017), with comparison to Ba* calculated from the South Atlantic dBa-dSi correlation in Horner et al. (2015) and a regional dBa-dSi correlation presented in Figure S6 of Supporting Information S1. In all plots, red squares, red circles, and blue triangles represent Congo River samples, surface FISH samples, and samples below the surface, respectively. In panel (a), the Atlantic data set is compiled from previously published δ^{138}Ba data from the Atlantic Ocean and the Atlantic Section of the Southern Ocean, including Horner et al. (2015), Bates et al. (2017), Hsieh and Henderson (2017), and Bridgestock et al. (2018). In panels (a and b), dashed lines represent linear regressions of surface water (red line), waters below the surface (blue line), and the Atlantic data set (gray line). In each regression, *K* represents the slope, and *R* represents the correlation. In panel (c), gray circles encompass plume samples with salinity lower than 32 and higher than 35. Arrows in panels (c and d) highlight the decoupling of Ba and Si.

Edmond et al., 1978). If we assume that the exchangeable Ba concentration in the Congo River is similar to that in other rivers (16–233 μg/g total suspended solid (TSS); see references in Bridgestock et al. (2021)), then the Congo River, which has a TSS load ranging between 10 and 30 mg/l (Coynel et al., 2005), contains ~0.16–7.00 μg/l exchangeable particulate Ba. The exchangeable particulate Ba flux is thus 0.2–9.1 Gg/yr at a discharge of 1.3×10^{12} m^3/year (Milliman & Farnsworth, 2011), which only accounts for a maximum of 43% of

Table 1
Ba and Si Fluxes of the Congo River (Stn. 12.1–12.3), the Congo-Shelf-Zone (Stn. 13–15), and the Off-Shelf 3°S Section (Stn. 17–24)

	Congo River	Congo-shelf-zone	Offshore 3°S transect
Ba-flux (mol/year)	$(1.68 \pm 0.09) \times 10^8$	$(5.54 \pm 2.31) \times 10^8$	$(3.07 \pm 1.09) \times 10^8$
Ba-flux (Gg/year)	23.11 ± 1.20	76.09 ± 31.71	42.19 ± 15.01
Si-flux (mol/year)	$(2.19 \pm 0.12) \times 10^{11}$	$(3.54 \pm 1.63) \times 10^{11}$	$(1.08 \pm 0.36) \times 10^{11}$
Si-flux (Tg/year)	6.16 ± 0.34	9.94 ± 4.58	3.05 ± 1.02

Note. See Section 2.3 for details on the calculation of Ba and Si fluxes based on ^{228}Ra.

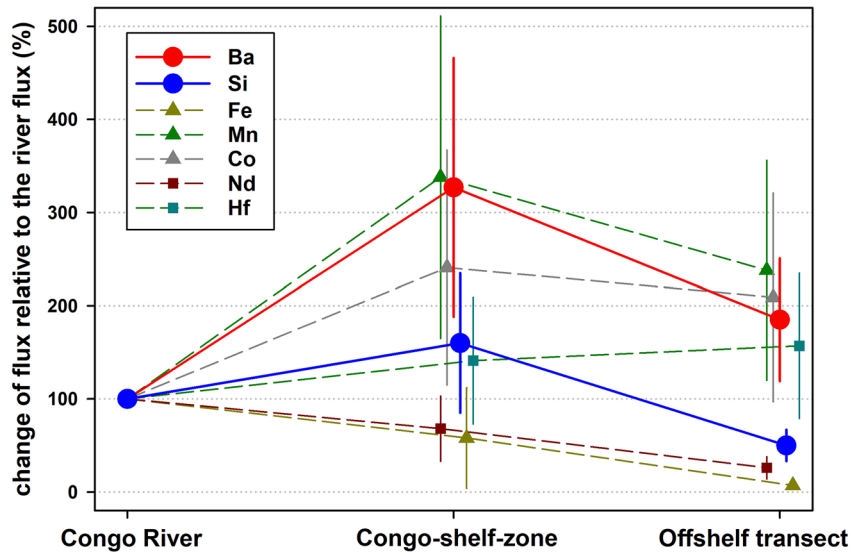

Figure 5. Relative changes of elemental fluxes of Ba, Si (circles, this study); Mn, Co, Fe (triangles, Vieira et al., 2020), and Nd, Hf (squares, Rahlf et al., 2021) from the Congo River to the Congo-shelf-zone and the off-shelf transect at 3°S.

the additional Ba input (53 ± 32 Gg/yr) into the Congo-shelf-zone. In the most extreme scenario with complete weathering and desorption of all particulate Ba from river-borne suspended particles, the particulate Ba flux (i.e., the maximum Ba release flux) is 10.3–30.8 Gg/yr based on the average Ba content of Congo River suspended matter (790 μg/g TSS, Martin & Meybeck, 1979). Therefore, even a high estimate of Ba release from particulates (including mineral weathering, dissolution, and desorption) cannot completely explain the increased Ba flux to the Congo-shelf-zone. This points to large additional Ba sources supplying the Congo-shelf-zone apart from the dBa release from riverine particles, such as SGD (Rahman et al., 2022; Whitmore et al., 2022) or diagenetic release from estuarine bottom sediments (Hong et al., 2018; Joung & Shiller, 2014).

When compared to the fluxes calculated for Fe, Mn, and Co (Vieira et al., 2020) and Nd and Hf (Rahlf et al., 2021), the increase of the Ba flux on the shelf closely resembles that of Mn, which also increases more than three-fold from the river to the shelf-zone (Figure 5). This suggests that the addition of Ba and Mn may originate from sources influenced by similar processes, for example, the reductive diagenetic release of Mn and Ba in the low oxygen estuarine/shelf sediment or the subterranean estuary (Charette & Sholkovitz, 2006; McManus et al., 1998), given that Ba has an exceptionally strong affinity to Mn (hydr)oxides (Balistrieri & Murray, 1986) and reductive Mn dissolution should thus release Ba. This is supported by the significant positive linear relationship between dBa and dissolved Mn (dMn) concentrations in the plume waters ($R^2 = 0.97$; Figure S4 in Supporting Information S1). In the Congo estuary, the remineralization of river-borne particulate organic carbon in sinking particles and stratification that reduces the vertical mixing of surface waters with waters below the pycnocline, leads to the presence of vast hypoxic and anoxic zones in the deep estuary (Eisma & van Bennekom, 1978; Vallaeys et al., 2021). McManus et al. (1998) pointed out that Ba preservation in shelf sediments is compromised under suboxic/anoxic conditions, which is closely associated with the cycling of manganese oxides. Hong et al. (2018) also found that the geochemical cycling of Ba in Pearl River estuarine sediments was closely linked to diagenetic reactions of manganese and iron oxides, and estimated high benthic fluxes of Ba into the overlying water column.

However, such Ba fluxes did not significantly impact the Ba isotopic signatures of the overlying water column during the same survey in the Pearl River estuarine (Cao et al., 2021). Indeed, based on the regression between δ^{138}Ba and salinity at salinities above 20 (Figure 3c),

$$\delta^{138}\mathrm{Ba} = \frac{-0.07(\pm 0.06) \times \mathrm{salinity} - 2.19(\pm 1.21)}{\mathrm{salinity} - 43.59(\pm 1.76)}$$

the effective Ba isotopic composition of the river water endmember ($\delta^{138}Ba_{eff}$) can be calculated by extrapolating the regression to zero salinity. The extrapolated $\delta^{138}Ba_{eff}$ values range between −0.01 and 0.11‰, which are consistent with the measured δ^{138}Ba values of the Congo River freshwater endmember ($\delta^{138}Ba_{river}$, 0.00–0.09‰).

This indicates that non-conservative Ba addition at low-mid salinities is characterized by Ba with a δ^{138}Ba signature similar to the corresponding riverine dBa pool. Previous studies have shown that estuarine processes modify the $\delta^{138}Ba_{river}$ of net riverine dBa fluxes toward lower values (0.2–0.3‰ lower), reflecting isotopic fractionation associated with the adsorption of Ba released during chemical weathering on land to mineral surfaces in the rivers (Bridgestock et al., 2021; Cao et al., 2021). However, such a pattern is not observed in this study. Global estimation suggested that the isotopic compositions of the fresh component of groundwater-derived Ba flux are isotopically indistinguishable from those of rivers (Mayfield et al., 2021). As such, input from porewater efflux or terrestrial SGD does not necessarily influence the Ba isotopic composition of the water column. In addition, we note that the Congo shows the lightest $\delta^{138}Ba_{river}$ signature amongst the rivers investigated so far (Table S1 in Supporting Information S1), which indicates that only minor fractionation of Ba isotopes, if any, occurs during solution-particle interaction in the Congo Basin.

3.1.2. Non-Conservative Addition of Si in the Congo-Shelf-Zone

Surface dSi concentrations generally decrease from the Congo River to the shelf, reflecting high riverine inputs to the coastal shelf area and subsequent mixing with surface seawaters (Figures 2 and 3; Figure S2 in Supporting Information S1). Riverine δ^{30}Si signatures display only a small inter-annual (May, July, and October) variability with a mean value of 1.19 ± 0.14‰ (1SD for the mean), which is comparable to the previously estimated δ^{30}Si signature of annual Si export (0.91‰) from the Congo River to the estuary between 2006 and 2008 (Hughes et al., 2011). The δ^{30}Si signatures of surface seawater (3.07 ± 0.16‰) are significantly heavier than the river waters. At high salinities above 32, a noticeable removal of dSi is observed, which corresponds to elevated δ^{30}Si signatures beyond the conservative mixing curve (Figure 3d). This observation points to a possible effect of diatom utilization at the edge of the Congo plume. This is consistent with a previous study that found maximum primary production at the plume edge (salinity ∼30) and dSi consumption at salinities higher than 30–32 in the Congo plume (Vangriesheim et al., 2009). Indeed, when plotting the δ^{30}Si values against inverse dSi concentrations, the data do not follow a clear linear trend (Figure S5 in Supporting Information S1), pointing to non-conservative processes other than simple two-endmember mixing with respect to δ^{30}Si. Instead, the surface waters are characterized by a linear relationship between δ^{30}Si values and logarithmic dSi concentrations ($R^2 = 0.87$, Figure 4b), reflecting Rayleigh-type fractionation during dSi utilization, which occurs in a closed system without further nutrient input from external sources (Reynolds et al., 2006). The gradient of the relationship between δ^{30}Si values and ln(dSi) would imply an apparent fractionation factor ($\Delta\delta^{30}$Si) of −0.42‰. This value is lower than previous estimates from culture studies (−0.54 to −2.09‰; De La Rocha et al., 1997; Sutton et al., 2013), implying that the observed relationship is also influenced by the mixing of other additional dSi sources into the system.

A striking feature of the surface water Si dynamics in the Congo River plume is the appreciable addition of dSi at mid-high salinities (∼20–32; Figure 3b), in contrast to the high utilization of Si by diatoms in other large river plumes (e.g., Amazon, Mississippi; Huang et al., 2012; Zhang, Cao, et al., 2020). This dSi addition is characterized by light δ^{30}Si signatures (Figure 3d). As shown in Figure 5 and Table 1, the Si flux to the Congo-shelf-zone increases to 160 (±75) % of the Congo River flux. Possible sources include the dissolution of river-borne particles such as amorphous silica (aSi, including bSi and highly reactive pedogenic silicates), inputs from SGD, and a benthic flux from shelf sediments near the river mouth (Tréguer et al., 2021). Due to the extreme weathering conditions prevailing in the Congo River Basin, river-borne TSS mainly consists of highly weathered clays (60%–80% kaolinite, 10%–15% illite) (Spencer et al., 2013). These are not prone to dissolution in seawater, as supported by the results of Jeandel and Oelkers (2015), who show that less than 0.1% of kaolinite and illite are expected to dissolve in seawater. Therefore, the dissolution of aSi in the Congo plume is mainly represented by the dissolution of bSi. A 2-year investigation of riverine δ^{30}Si close to the Congo River mouth revealed a linear relationship between measured riverine δ^{30}Si values and bSi concentrations ($R^2 = 0.93$; Hughes et al., 2011):

$$\delta^{30}\mathrm{Si} = 0.03 \times \mathrm{bSi} + 0.70$$

Thus, we estimate the river-borne bSi concentration at the time of our sampling to be 16.4 (±4.6) μM based on the riverine δ^{30}Si value of 1.19 ± 0.14‰. This represents 8.9 (±2.5)% of the total Si pool (bSi + dSi), which is consistent with the previously estimated contribution of bSi to the total Si pool exported from the Congo River to the estuary (∼5.1% annually, 0.5%–26.9% monthly, Hughes et al., 2011). Dissolution of river-borne bSi therefore only contributes to a small fraction of the 60% increase of the Si flux. Therefore, SGD or shelf sediments are more likely the main contributors of the additional Si flux to the shelf zone. Despite lacking information on

the SGD flux on the Congo shelf, SGD has been recently estimated to be the second largest source of dSi to the global ocean (Rahman et al., 2019). Terrestrial SGD generally contributes Si with lighter δ^{30}Si signatures (mean of 0.19‰) than that of rivers and coastal seawaters (Frings et al., 2016), which is consistent with our observation of additional light δ^{30}Si input. Growing evidence has shown that the porewater efflux of Si is a significant source of Si at coastal margins (Percuoco et al., 2015; Raimonet et al., 2013; Tallberg et al., 2017), although the Si isotopic signature of the benthic Si flux shows large variability across different regions (Geilert et al., 2020; Ng et al., 2020; Ward et al., 2022).

To summarize, the flux of Ba increases by more than a factor of three (addition of 53 ± 32 Gg/yr) along the Congo River plume's pathway across the shelf zone, while the Si flux only increases by 60% (±75%) from the Congo River flux. Despite the significant additional dBa input, δ^{138}Ba values in surface waters with salinities above 20 demonstrate conservative mixing. On the other hand, the dSi addition is characterized by light δ^{30}Si signatures. These additional inputs mainly result from river-borne particle desorption or dissolution and shelf inputs (SGD or porewater efflux).

3.1.3. Decoupled Behavior of Ba and Si in the Congo River Plume

As a result of riverine inputs with light isotopic signatures, the surface water δ^{138}Ba and δ^{30}Si distributions both display a general increase along the flow path of the plume. However, gradients in surface water δ^{138}Ba and δ^{30}Si are notably different within the plume (Figures 2 and 3). Marked lighter δ^{30}Si signatures (~2‰) than those of the open-ocean (~3‰) still prevail along the off-shelf transect at 4°S until ~4°E, whereas δ^{138}Ba values are similar to those of the open-ocean (~0.6‰) close to the Congo-shelf-zone.

Plots of δ^{138}Ba versus δ^{30}Si and δ^{138}Ba versus Ba* reveal distinct differences between the geochemical behavior of Ba and Si (Figures 4c and 4d). In the surface waters, two major deviations from the overall positive δ^{138}Ba-δ^{30}Si correlation are evident (Figure 4c). First, δ^{138}Ba and δ^{30}Si show a slight negative correlation in the Congo-shelf-zone (purple arrow). δ^{30}Si values decrease as a result of the additional contributions from a source carrying light δ^{30}Si signatures. At the same time, δ^{138}Ba signatures are not affected by such a light source but instead increase as a function of increasing the admixture of isotopically heavy seawater. Second, along the off-shelf transect, δ^{30}Si values continue to increase (from 2 to 3‰) whereas δ^{138}Ba values stay constant (~0.6‰) (green arrow). This indicates that during off-shelf transport, dSi is progressively depleted and likely fractionated biologically, whereas dBa is not further removed and fractionated in the surface waters due to a lack of significant uptake processes. Ba* values increase significantly from the Congo River (−10 to −20) to the shelf surface waters (10–20) (Figure 4d), reflecting a stronger enrichment of Ba than Si during estuarine mixing. When excluding the river data, Ba* and δ^{138}Ba have an overall negative linear relationship as a result of mixing between the dBa enriched (relative to dSi) and isotopically light shelf waters and typical isotopically heavy open ocean surface waters (Ba* ~0).

3.1.4. Comparison With the Amazon River Plume

The Amazon and Congo rivers are the two largest rivers in the world in terms of freshwater discharge and both greatly impact the biogeochemistry of the tropical Atlantic and beyond (Nittrouer & DeMaster, 1996). Therefore, we compare the signatures of Ba and Si isotopes and their controlling mechanisms in the Congo and Amazon plumes. Previously published datasets of δ^{30}Si (Zhang, Cao, et al., 2020) and δ^{138}Ba (Bridgestock et al., 2021) from the Amazon River plume are used for this comparison.

Si dynamics in the Amazon plume are substantially different from those in the Congo plume (Figure 3). Significant Si isotopic fractionation due to diatom growth was observed over the entire salinity range in the Amazon plume during two different sampling seasons (February 2012, May 2018; Zhang, Cao, et al., 2020). The contrast between these two plumes results from the large difference in diatom productivity: the Amazon plume supports much higher primary production and stronger diatom blooms (Cadée, 1978). Primary production in the Congo River plume reaches values hardly above those in the oceanic surface waters outside the plume but is one order of magnitude higher in the Amazon River plume than in the adjacent ocean (Cadée, 1978). For instance, surface chlorophyll-a (Chl-a) concentrations in the Congo River plume are overall lower than ~2 μg/l across different seasons (Cadée, 1978, 1984; Hopkins et al., 2013). In comparison, surface Chl-a concentrations in the Amazon River plume are an order of magnitude higher (up to 10–12 μg/l (DeMaster et al., 1996; Zhang, Cao, et al., 2020)). The underlying reasons for the contrasting productivity between these two plumes have been discussed in detail by Cadée (1978). In brief, most of the terrigenous sediment from the Amazon River settles out at low salinities due

to strong vertical mixing driven by extensive shoaling before the river mouth. The rapid turbidity drop increases the incident light at the surface and favors diatom growth in the middle salinity range where the nutrient level remains high. In contrast, the deep canyon of the Congo estuary rapidly channels freshwater as a thin layer into the ocean whereby the isohalines stay nearly horizontal, and terrigenous sediment remains in suspension at higher salinities in the estuary. This gives rise to much later development of the diatom bloom at much higher salinities where nutrient levels are already too low to sustain significant diatom production. As such, the strong diatom bloom that is present throughout the year in the Amazon plume leads to significantly elevated δ^{30}Si values beyond conservative mixing (Figure 3d, Zhang, Cao et al., 2020). In contrast, the lack of significant diatom production in the Congo plume allows the detection of Si inputs from the shelf based on their light δ^{30}Si signatures.

Unlike Si, Ba behaves similarly in the Amazon and Congo plumes (Figure 3). Surface dBa concentrations in the Amazon River plume are generally higher despite similar dBa_{river} concentrations of both rivers. Given that the primary source of the released Ba during estuary mixing is the fresh river-borne materials (Coffey et al., 1997), the magnitude of Ba release strongly depends on the riverine supply of particulate matter (Samanta & Dalai, 2016). Sediment discharge of the Amazon River (1,200 Mt/yr) is two orders of magnitude higher than that of the Congo River (43 Mt/yr) (Milliman & Farnsworth, 2011). The much higher ratio of sediment flux to water flux of the Amazon River (190 g/m^3) than that of the Congo River (33 g/m^3) leads to a larger desorption flux of Ba in the low salinity zone of the Amazon River plume (Samanta & Dalai, 2016). However, despite their different dBa concentrations, the δ^{138}Ba signatures are overall comparable between the two plumes (Figure 3). This indicates that diatom silica production only has a minor effect on dissolved Ba isotopic compositions in large river plumes, which agrees well with laboratory observations demonstrating that diatoms do not incorporate Ba in significant amounts (Sternberg et al., 2005). Admittedly, the δ^{138}Ba and δ^{30}Si datasets of the Amazon River plume were not obtained from the same samples and the same cruise. Seasonal variations of bSi standing stock and the average primary production rate in the optimal-growth zone are small (DeMaster et al., 1996). δ^{30}Si values also display similar patterns in different seasons, indicating invariable Si isotope fractionation processes (Zhang, Cao, et al., 2020). It is therefore reasonable to assume that the Si dynamics during the cruise on which the samples for δ^{138}Ba measurements were obtained (Bridgestock et al., 2021) were similar to those reported by Zhang, Cao, et al. (2020).

In summary, Si dynamics in the Amazon plume are substantially different from those in the Congo plume, and the δ^{30}Si values in the Amazon plume are significantly elevated beyond conservative mixing due to the strong diatom silica production. In contrast, Ba behaves similarly in the Amazon and Congo plumes and their δ^{138}Ba signatures are overall comparable, indicating that diatom silica production has a negligible effect on dissolved Ba isotopic compositions in large river plumes.

3.2. Decoupling of Ba and Si in the Epipelagic and Mesopelagic Layers

The vertical profiles document clear and systematic changes in dBa, dSi, δ^{138}Ba, δ^{30}Si, and Ba* in the subsurface waters across all stations from the shelf to the northern Angola Basin (Figure 6). Ba and Si are decoupled in both the epipelagic (0–200 m water depth) and mesopelagic (200–1,000 m water depth) layers. Except for those surface waters that are influenced by the river plume (Salinity <35), dBa concentrations are low and δ^{138}Ba values are high and essentially invariant in the epipelagic layer (0–200 m), whereas dSi gradually decreases and δ^{30}Si values progressively increase in the surface water. This supports the lack of Ba uptake and barite precipitation in the euphotic zone where organic matter production prevails over degradation. On the other hand, silicifiers, particularly diatoms, consume dSi and preferentially incorporate lighter Si isotopes, resulting in an enrichment of the surface waters in heavy Si isotopes. This is also reflected by a drastic decrease of Ba* values from ~2 at the surface to ~−5 at 200 m depth (*t*-test of significant difference, $p = <0.001$).

In the mesopelagic layer (200–1,000 m), the thermocline nutrients are supplied by Eastern South Atlantic Central Waters (ESACW, 100–500 m) and Antarctic Intermediate Water (AAIW, 500–1,000 m) (Text S1 in Supporting Information S1; Rahlf et al., 2021). The formation area of ESACW is located in the area southwest of South Africa and south of the Benguela Current (30°–40°S, 0°–20°E), while AAIW originates from the surface region north of the Antarctic Circumpolar Current (Liu & Tanhua, 2021; Peterson & Stramma, 1991). Both water masses are characterized by more positive Ba* values due to the efficient Si removal in the surface water of the Polar Front Zone (Bates et al., 2017; Horner et al., 2015). For example, Ba* values range between 3 and 9 in the upper 1,000 m at a station located in the ESACW formation area (Sta.6 in Horner et al. (2015)). As shown in Figure 7c,

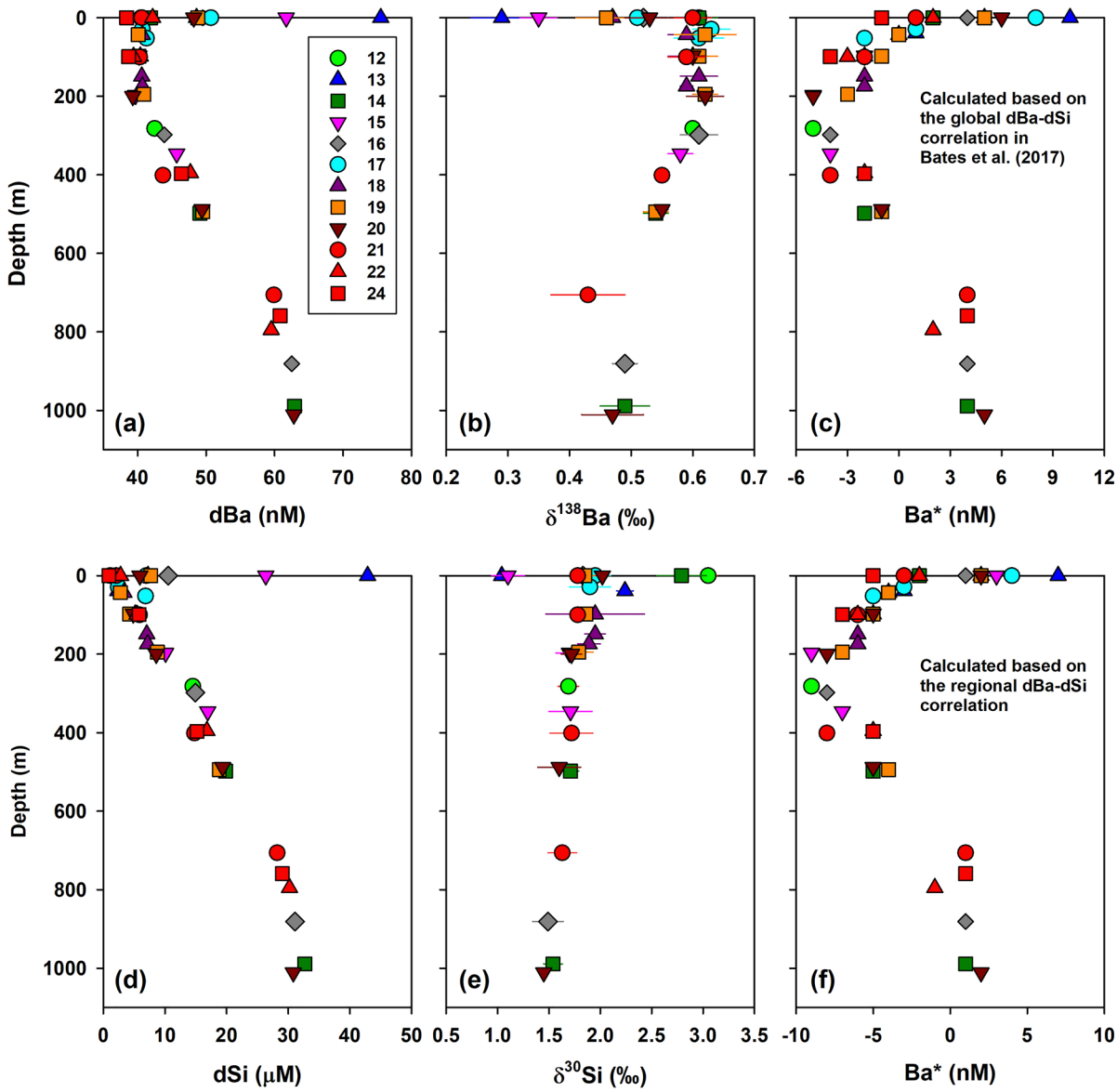

Figure 6. Depth profiles of (a) dBa, (b) δ^{138}Ba, (c) Ba* calculated based on the global dBa-dSi correlation in Bates et al. (2017), (d) dSi, (e) δ^{30}Si and (f) Ba* calculated based on the regional dBa-dSi correlation in this study at stations 12–24.

Ba* values in the mesopelagic layer decrease markedly from that location (~3–9, green triangle) to our study site (~−5 to 5, red triangles), likely reflecting both the in situ removal of Ba, superimposed atop the progressive depletion of Ba during the northward transport of the Si-poor ESACW and AAIW. δ^{138}Ba signatures become heavier from the base of the thermocline (1,000 m, δ^{138}Ba ~ 0.49‰) to the upper mesopelagic layer (200 m, δ^{138}Ba ~ 0.60‰), likely as a result of in situ barite precipitation in the twilight zone which favors the incorporation of isotopically light Ba and leads to isotopically heavy residual Ba in the ambient water (Horner et al., 2015). In contrast, δ^{30}Si values display insignificant variations in this layer (*t*-test of significant difference, $p = 0.333$). Strikingly, δ^{138}Ba signatures show no variations across all shelf stations in the twilight zone (Figure 6b), even though the surface salinity (Figure 3) and in situ primary production (Cadée, 1978) exhibit a large variability under the influence of the Congo River plume. This reveals the dominant control of ocean circulation and water mass mixing on the Ba distribution in the subsurface water on the Congo shelf.

In summary, Ba and Si show decoupling in both the epipelagic and mesopelagic layers, likely due to differing depths of in situ barite precipitation and biogenic silica production. Homogeneous Ba concentrations and isotope

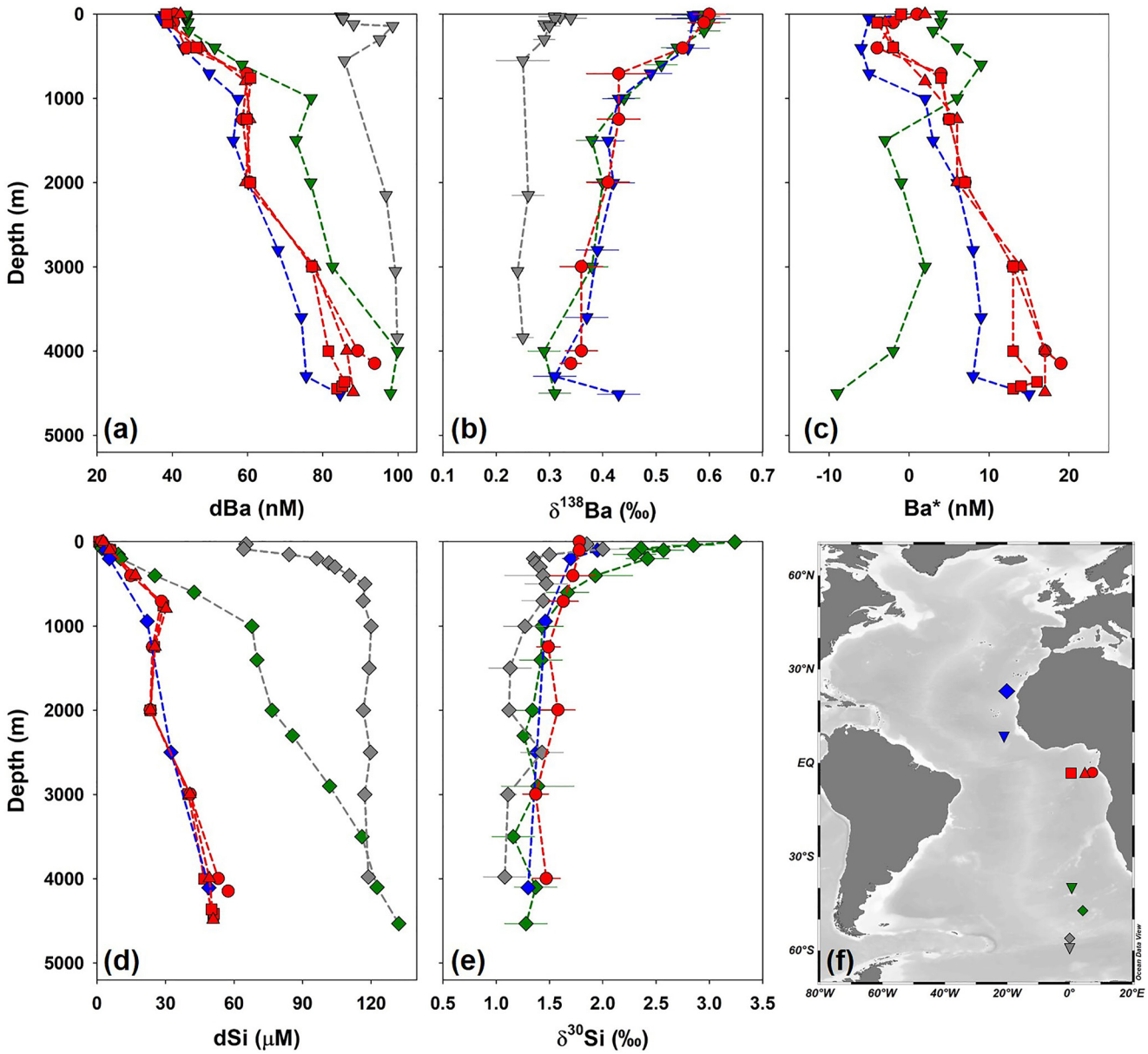

Figure 7. Compiled depth profiles of (a) dBa, (b) δ^{138}Ba, (c) Ba*, (d) dSi, and (e) δ^{30}Si at off-shelf stations (red symbols; Stn. 21-circle, Stn. 23-triangle, Stn. 24-square) in this study, along with previously published Ba (triangle down) and Si (diamond) profiles in the northeastern Atlantic Ocean (blue symbols), southeastern Atlantic Ocean (green symbols), and Southern Ocean (gray symbols). Panel (f) displays a map of all compiled stations. The Ba data set is compiled from Stn. 2 (9°N, 21°W) in Bates et al. (2017), S5 (58°S, 0°E) in Hsieh and Henderson (2017), and Stn. 6 (40°S, 1°E) in Horner et al. (2015); Si data set from PS69/11 (23°N, 21°W) in De Souza, Reynolds, Rickli, et al. (2012) and Super3 (47°S, 4°E), Super5 (57°S, 0°E) in Fripiat et al. (2011). Ba* values in this plot are calculated based on the global dBa-dSi correlation in Bates et al. (2017). A comparison to Ba* calculated from the South Atlantic dBa-dSi correlation applied by Horner et al. (2015) and the regional dBa-dSi correlation in this study can be found in Figure S7 of Supporting Information S1, which shows the insignificant influence of the different equations on the resulting vertical Ba* variation.

compositions in the epipelagic layer reflect the absence of Ba removal, while the enrichment of heavy Si isotopes in the surface results from the biological consumption of Si. In the mesopelagic layer, in situ barite precipitation and the progressive depletion of Ba during the northward transport of Si-poor water masses lead to a decrease in Ba* values.

3.3. Decoupling of Ba and Si in the Deep and Bottom Waters

To disentangle the role of ocean circulation and local-scale inputs from the ocean boundaries in regulating Ba and Si dynamics in the deep water of the northern Angola Basin, we compare the vertical distributions of Ba

and Si at off-shelf stations (Figure 7, red symbols) with representative profiles of the Atlantic Ocean. Generally, deep waters of the northern Angola Basin below 2,000 m are dominated by North Atlantic Deep Water (NADW) because there is little entrainment of Antarctic Bottom Water (AABW) into the northern Angola Basin due to topographic barriers (Text S1 in Supporting Information S1; Rahlf et al., 2021). However, significantly elevated dBa concentrations compared to those in the northeastern Atlantic are observed below 3,000 m water depth (Figure 7a, blue triangle down). In contrast, dSi concentrations in deep and bottom waters are similar to those in the northeastern Atlantic (Figure 7d, blue squares) but are slightly elevated at the station closest to the shore (Stn. 21). Ba* values (Figure 7c, red symbols) are substantially elevated in the Angola Basin compared to those in the North Atlantic (blue triangle down) and South Atlantic (green triangle down), documenting that these are not controlled by mixing between the North-sourced and South-sourced deep water masses. The Angola Basin is a restricted basin and the age of the deep-water mass is relatively high (~1,000 years of radiocarbon age, Matsumoto, 2007), which favors increased barite dissolution and Si remineralization. However, the enrichment of dBa compared to dSi also points to a regional source with a higher Ba/Si ratio than the global seawater average.

Non-conservative additions of dBa (dBa_{ncon}) in the deep waters below 2,000 m are identified as the deviations of measured dBa from the concentrations expected from conservative dBa (dBa_{con}). The latter can be calculated based on conservative mixing of two deep-water endmembers: AABW and NADW:

$$f_{AABW} + f_{NADW} = 1 \quad (1)$$

$$\text{Salinity} = \text{Salinity}_{AABW} \times f_{AABW} + \text{Salinity}_{NADW} \times f_{NADW} \quad (2)$$

$$dBa_{con} = dBa_{AABW} \times f_{AABW} + dBa_{NADW} \times f_{NADW} \quad (3)$$

where dBa_{AABW} and dBa_{NADW} denote the end-member dBa in AABW and NADW, and f_{AABW} and f_{NADW} are the percent contribution of AABW and NADW for the deepwater in the Angola Basin based on salinity. Adopting salinity and dBa concentrations of AABW (Salinity = 34.66, dBa = 103 ± 10 nM) and NADW (Salinity = 35.00, dBa = 51 ± 5 nM) endmembers in Hsieh and Henderson (2017), non-conservative additions of dBa are estimated to be ~10–25 nM in the deep waters below 2,000 m (Figure S8 in Supporting Information S1) based on the following equation:

$$dBa_{ncon} = dBa_{meas} - dBa_{con} \quad (4)$$

where dBa_{meas} denotes the observed dBa concentration. The bottom water at Stn. 21 contains the largest non-conservative Ba addition of 23.4 ± 4.9 nM, corresponding to a 33% increase compared to the expected conservative dBa level.

Both Ba* and non-conservative dBa in the deep/bottom waters (~4,000 m) increase gradually toward the African shelf (from Stn. 24 to 21; Figure 7c and Figure S8 in Supporting Information S1), reflecting possible inputs from the continental margin. Congo-derived suspended particles have limited influence on Ba chemistry in deep waters of the Angola Basin because Ba desorption from Congo-derived suspended particles occurs as soon as the river water mixes with seawater, as revealed by the conservative mixing of dBa in the surface waters at high salinities (Section 3.1.1). Enhanced ^{223}Ra, ^{226}Ra, and ^{228}Ra activities (0.029, 21.00, 0.88 dpm 100 L^{-1}) were observed in the bottom water above the seafloor compared to a depth of ~4,000 m (0.019, 17.12, 0.21 dpm 100 L^{-1}), pointing to abyssal inputs from the sediment (Vieira, 2019). Similarly, the enrichment of dissolved REE concentrations with less radiogenic Nd isotopic values has also been observed in the deep and bottom waters of the northern Angola Basin (same study site as in this study; Rahlf et al., 2021) and the central Angola Basin (Rahlf et al., 2020; Zheng et al., 2016), which were largely attributed to the release of REE and Nd from suboxic surface sediments and remineralization of sinking particles. Previous studies have also observed dBa excess below 2,000 m at the Portuguese coast off Lisbon during the GEOTRACES GA01 cruise (Le Roy et al., 2018), as well as along the broad Mauritanian shelf (Rahman et al., 2022), which likely originated from benthic inputs and barite dissolution in the deep water. Assuming that dissolution of sinking pelagic barite contributes most of the non-conservative addition of dBa in the northern Angola Basin, the deep-sea $\delta^{138}Ba$ signatures (red circle, Figure 7b) are expected to become lighter than in the North Atlantic (blue triangle down, Figure 7b) given that barite has a much lighter $\delta^{138}Ba$ signature (~0–0.1‰; Horner et al., 2021) than the Atlantic deep waters (~0.3–0.4‰). This is not confirmed by the $\delta^{138}Ba$ versus Ba* plot, where $\delta^{138}Ba$ values of deep and bottom water do not follow the overall negative trend (Figure 4d, orange arrow). With a known source of non-conservative Ba, deep-sea $\delta^{138}Ba$ signatures can thus be estimated ($\delta^{138}Ba_{est}$) based on the equations:

$$F_{con} + F_{ncon} = 1 \quad (5)$$

$$dBa_{meas} = dBa_{con} \times F_{con} + dBa_{ncon} \times F_{ncon} \quad (6)$$

$$\delta^{138}Ba_{con} = \frac{\delta^{138}Ba_{AABW} \times dBa_{AABW} \times f_{AABW} + \delta^{138}Ba_{NADW} \times dBa_{NADW} \times f_{NADW}}{d\,Ba_{con}} \quad (7)$$

$$\delta^{138}Ba_{est} = \frac{\delta^{138}Ba_{con} \times dBa_{con} \times F_{con} + \delta^{138}Ba_{ncon} \times dBa_{ncon} \times F_{ncon}}{dBa_{meas}} \quad (8)$$

where $\delta^{138}Ba_{AABW}$ (0.25‰) and $\delta^{138}Ba_{NADW}$ (0.45‰) denote the end-member $\delta^{138}Ba$ in AABW and NADW adopted from Hsieh and Henderson (2017), and F_{con} and F_{ncon} are the percent contributions of dBa_{con} and dBa_{ncon} to the deepwater in the Angola Basin based on dBa concentration. Even assuming the barite $\delta^{138}Ba$ signature as 0.1‰, $\delta^{138}Ba$ at Stn. 21, for example, is calculated to range between 0.20 and 0.27‰, which is lighter than our measured signatures (0.34–0.36‰; red circle, Figure 7b). This indicates that the dissolution of sinking pelagic barite is not the main source of the non-conservative addition of dBa.

Benthic input may provide an alternative explanation. Significantly elevated dBa and Ba* values were previously observed in the tropical North Atlantic bottom waters corresponding to a slight deviation toward heavier $\delta^{138}Ba$ which were attributed to a significant sedimentary influence on dBa in bottom waters (Bates et al., 2017). At the Congo margin, the deep-water enrichments of both dBa and dSi may be associated with enhanced benthic inputs from the Congo submarine canyon-channel-deep-sea fan system. A large volume of the Congo discharged bedload sediments is carried by turbidity currents to the Congo deep-sea fan via the submarine canyon (Savoye et al., 2009). Organic matter and amorphous silica in the deep-sea lobe complex are dominated by the canyon inputs, rather than pelagic sinking particles (Rabouille et al., 2019). Previous studies have observed decreases in oxygen and increases in nutrient concentrations in deep waters (~4,000 m depth) at the Congo margin, attributable to the oxidation of particulate organic matter either from the Congo channel during turbidity current events (Braga et al., 2004; Vangriesheim et al., 2009) or downslope particle transport (Ragueneau et al., 2009). The benthic flux of dSi was estimated to be 0.61 mol Si m^{-2} yr^{-1} in the vicinity of the Congo submarine deep channel at 4,000 m depth (Ragueneau et al., 2009) and 0.30 ± 0.06 mol Si m^{-2} yr^{-1} from the terminal lobes of the Congo deep-sea fan (Raimonet et al., 2015). These fluxes are one order of magnitude higher than those from the Northeast Atlantic (0.017 mol Si m^{-2} yr^{-1}) (Ragueneau et al., 2001), Northwest Atlantic (0.057 mol Si m^{-2} yr^{-1}) (Sayles et al., 1996), and average benthic efflux from non-siliceous deep-sea sediments (~0.010–0.020 mol Si m^{-2} yr^{-1}) (Tréguer et al., 2021).

Although no investigations into the benthic flux of Ba from the channel and deep-sea fan sediments have been reported so far, recent investigations of early diagenesis in the Congo deep-sea fan sediments within the CONGOLOBE project have shed light on potential high benthic dBa flux. The tremendous amounts of labile organic and inorganic material from the Congo River that fed into the deep-sea fan led to either high oxygen consumption and reducing conditions in the sediments (Pozzato et al., 2017) or active anaerobic benthic respiration dominated by dissimilatory iron reduction (Taillefert et al., 2017) or sulfate reduction and methanogenesis (Pastor et al., 2017). The intense metal-reducing or sulfate-reducing conditions are more similar to those in a coastal system than in a deep-sea environment, which may facilitate a high benthic Ba flux via the dissolution of barite or reductive release of Ba from Fe/Mn (hydr)oxides (Hong et al., 2018; Joung & Shiller, 2014). Although Scholz et al. (2023) recently found that the benthic Ba flux leads to enrichment of isotopically light Ba in the deep waters of Kiel Bight, the Baltic Sea, the isotopic signature of the benthic Ba input is still poorly constrained due to limited data from other settings. Future research should focus on investigating Ba isotope fractionation in sediments and porewaters from different seafloor environments to obtain a better understanding of the isotopic signatures and contributions of the Ba benthic flux to deep waters.

In summary, our analysis reveals significant non-conservative enrichments of dBa in the deep waters (below 3,000 m) of the northern Angola Basin, as evidenced by deviations of measured dBa from concentrations expected during conservative mixing. These enrichments are likely driven by benthic inputs of dBa from the terrigenous sediments that feed the Congo canyon-deep sea fan system.

3.4. Global Implications

This work highlights the strong marginal influence on the Ba cycle at the Congo margin (Figure 8), which was also recently observed in other margin regions globally, for example, in the Arctic Ocean (Whitmore et al., 2022) and along the broad Mauritanian shelf (Rahman et al., 2022). Adopting the estimated global freshwater dBa river input (6.6 ± 3.9 Gmol/yr; Rahman et al., 2022), the Congo River dBa flux accounts for 2.5 ± 1.5% of this global estimation.

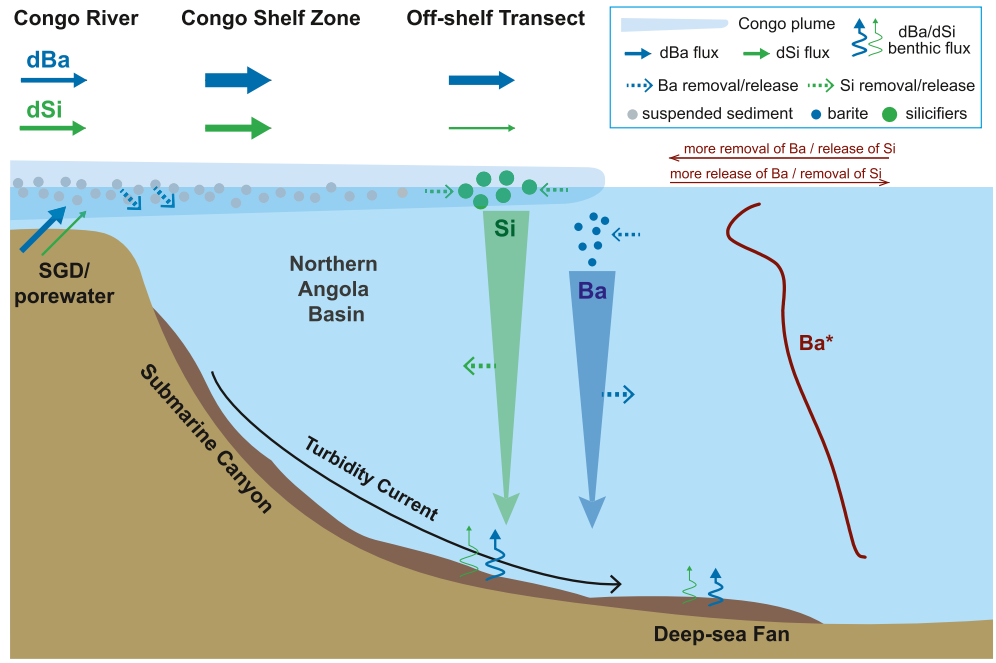

Figure 8. This conceptual figure illustrates the decoupling of Ba and Si at the Congo margin. The thickness of the solid line arrows represents the changes in the fluxes of dBa and dSi from the Congo River to the Congo-shelf-zone and the off-shelf transect. Arrows representing dBa and dSi fluxes from the Congo River are normalized to 1:1 thickness. The vertical profile of Ba* indicates the decoupling of Ba and Si, and is based on data collected from Stn. 21.

Estuarine mixing processes and shelf inputs add another 0.39 ± 0.23 Gmol/yr Ba to the Congo-shelf-zone, which is equivalent to 5.9% ± 4.9% of the global freshwater input. According to our data, at least half of this additional input is contributed by the shelf, including SGD or sedimentary inputs. Adopting the estimated global riverine Si flux (8.1 ± 2.0 Tmol/yr; Tréguer et al. (2021)) which already takes into consideration the dissolution of amorphous silica, the Congo-shelf-zone Si flux accounts for 4.4% ± 2.3% of the global flux. Even though the observed Ba flux dropped by 44% ± 31% and the Si flux dropped by 69% ± 18% from the Congo-shelf-zone to the 3°S off-shelf transect, mainly due to the admixture of seawater (Table 1). Still, the off-shelf export of Congo-derived Ba and Si along the 3°S transect is markedly high with enriched concentrations relative to seawater extending for up to 1,000 km offshore. High freshwater discharge, as well as large additional inputs into the Congo-shelf-zone thus sustain significant off-shelf transport of dBa and dSi to the oligotrophic Atlantic surface ocean. In addition, the strong enrichment of dBa in the deep water of the northern Angola Basin, likely associated with the benthic input from reducing sediments, also highlights the strong margin influence on the Ba cycle. In light of these findings, marginal inputs of Ba to shelf waters and the open ocean will likely change at a faster rate than those of Si in the future ocean with intensifying ocean deoxygenation. Further investigations of the benthic Ba cycle, particularly in hypoxic/anoxic environments and their associated redox conditions, will allow us to better reconstruct the Ba dynamics in the past and predict it in the future.

This work also reveals a pronounced decoupling of Ba and Si at a river-dominated continental margin, where local processes and boundary inputs largely override the dominant control of ocean circulation (Figure 8). Based on the observations that (a) δ^{138}Ba behave similarly between the Congo and Amazon plumes despite the large differences in their δ^{30}Si distributions induced by contrasting diatom productivity and (b) dSi consumption and dBa removal occur at different depths in the upper ocean of the northern Angola Basin, we conclude that Ba and Si are controlled by fundamentally different biogeochemical processes. These findings strongly suggest that the main process controlling the global correlation of dBa and dSi concentrations is large-scale ocean circulation rather than concurrent biological processes.

4. Conclusions

Our combined measurements of stable Ba and Si isotopes together with the estimation of Ba and Si fluxes based on ^{228}Ra reveal a pronounced decoupling of Ba and Si in the Congo River-dominated Southeast Atlantic margin.

Compared to the Si flux, the Ba flux shows more prominent amplification along the plume pathway from the Congo River to the shelf zone, mainly caused by large shelf inputs (SGD or porewater efflux) and river-borne particle desorption. In addition, the dSi flux decreases drastically in the off-shelf region due to consumption by diatoms at the edge of the plume, whereas the Ba flux only decreases as a consequence of dilution given that it is not significantly influenced by diatom production. Ba and Si are also decoupled in the epipelagic and mesopelagic layers, likely due to different depth intervals of in situ barite precipitation and biogenic silica production. Deep water (below 3,000 m) enrichments of dBa are observed in the northern Angola Basin, likely associated with benthic inputs fed by terrigenous sediments of the Congo canyon-deep sea fan system.

Conflict of Interest

The authors declare no conflicts of interest relevant to this study.

Data Availability Statement

Maps and figures were produced using Ocean Data View, and Sigmaplot. All data presented in this study have been included in the Supporting Information (data table). All data are publicly available on PANGAEA (https://doi.pangaea.de/10.1594/PANGAEA.956054).

Acknowledgments
We thank the captain and crew of RV Meteor for their help and support during cruise M121 (GEOTRACES cruise GA08). We also thank Jutta Heinze and Marcus Gutjahr for laboratory support. We are highly grateful to Bomba Sangolay (Instituto Nacional de Investigacao Pesqueira, Luanda, Angola) and his colleagues for the Congo River water sampling. We would like to thank the editor and two anonymous reviewers for their constructive comments on a previous version of the manuscript.

References

Bacon, M. P., & Edmond, J. M. (1972). Barium at Geosecs III in the southwest Pacific. *Earth and Planetary Science Letters*, *16*(1), 66–74. https://doi.org/10.1016/0012-821X(72)90237-3

Balistrieri, L. S., & Murray, J. W. (1986). The surface chemistry of sediments from the Panama Basin: The influence of Mn oxides on metal adsorption. *Geochimica et Cosmochimica Acta*, *50*(10), 2235–2243. https://doi.org/10.1016/0016-7037(86)90078-5

Bates, S. L., Hendry, K. R., Pryer, H. V., Kinsley, C. W., Pyle, K. M., Woodward, E. M. S., & Horner, T. J. (2017). Barium isotopes reveal role of ocean circulation on barium cycling in the Atlantic. *Geochimica et Cosmochimica Acta*, *204*, 286–299. https://doi.org/10.1016/j.gca.2017.01.043

Braga, E. S., Andrié, C., Bourlès, B., Vangriesheim, A., Baurand, F., & Chuchla, R. (2004). Congo River signature and deep circulation in the eastern Guinea Basin. *Deep-Sea Research Part I Oceanographic Research Papers*, *51*(8), 1057–1073. https://doi.org/10.1016/j.dsr.2004.03.005

Bridgestock, L., Hsieh, Y. T., Porcelli, D., Homoky, W. B., Bryan, A., & Henderson, G. M. (2018). Controls on the barium isotope compositions of marine sediments. *Earth and Planetary Science Letters*, *481*, 101–110. https://doi.org/10.1016/j.epsl.2017.10.019

Bridgestock, L., Nathan, J., Paver, R., Hsieh, Y.-T., Porcelli, D., Tanzil, J., et al. (2021). Estuarine processes modify the isotope composition of dissolved riverine barium fluxes to the ocean. *Chemical Geology*, *579*, 120340. https://doi.org/10.1016/j.chemgeo.2021.120340

Cadée, G. C. (1978). Primary production and chlorophyll in the Zaire River, estuary and plume. *Netherlands Journal of Sea Research*, *12*(3/4), 368–381. https://doi.org/10.1016/0077-7579(78)90040-6

Cadée, G. C. (1984). Particulate and dissolved organic carbon and chlorophyll A in the Zaire river, estuary and plume. *Netherlands Journal of Sea Research*, *17*(2–4), 426–440. https://doi.org/10.1016/0077-7579(84)90059-0

Cao, Z., Li, Y., Rao, X., Yu, Y., Hathorne, E. C., Siebert, C., et al. (2020). Constraining barium isotope fractionation in the upper water column of the South China Sea. *Geochimica et Cosmochimica Acta*, *288*, 120–137. https://doi.org/10.1016/j.gca.2020.08.008

Cao, Z., Rao, X., Yu, Y., Siebert, C., Hathorne, E. C., Liu, B., et al. (2021). Stable barium isotope dynamics during estuarine mixing. *Geophysical Research Letters*, *48*(19), 1–11. https://doi.org/10.1029/2021GL095680

Cao, Z., Siebert, C., Hathorne, E. C., Dai, M., & Frank, M. (2016). Constraining the oceanic barium cycle with stable barium isotopes. *Earth and Planetary Science Letters*, *434*, 1–9. https://doi.org/10.1016/j.epsl.2015.11.017

Carter, S. C., Paytan, A., & Griffith, E. M. (2020). Toward an improved understanding of the marine barium cycle and the application of marine barite as a paleoproductivity proxy. *Minerals*, *10*(5), 1–24. https://doi.org/10.3390/min10050421

Chan, L. H., Drummond, D., Edmond, J. M., & Grant, B. (1977). On the barium data from the Atlantic GEOSECS expedition. *Deep-Sea Research*, *24*(7), 613–649. https://doi.org/10.1016/0146-6291(77)90505-7

Charette, M. A., Lam, P. J., Lohan, M. C., Kwon, E. Y., Hatje, V., Jeandel, C., et al. (2016). Coastal ocean and shelf-sea biogeochemical cycling of trace elements and isotopes: Lessons learned from GEOTRACES. *Philosophical Transactions of the Royal Society A: Mathematical, Physical & Engineering Sciences*, *374*(2081), 20160076. https://doi.org/10.1098/rsta.2016.0076

Charette, M. A., & Sholkovitz, E. R. (2006). Trace element cycling in a subterranean estuary: Part 2. Geochemistry of the pore water. *Geochimica et Cosmochimica Acta*, *70*(4), 811–826. https://doi.org/10.1016/j.gca.2005.10.019

Cho, H. M., Kim, G., Kwon, E. Y., Moosdorf, N., Garcia-Orellana, J., & Santos, I. R. (2018). Radium tracing nutrient inputs through submarine groundwater discharge in the global ocean. *Scientific Reports*, *8*(1), 4–10. https://doi.org/10.1038/s41598-018-20806-2

Chow, T. J., & Goldberg, E. D. (1960). On the marine geochemistry of barium. *Marine Chemistry*, *20*(3–4), 192–198. https://doi.org/10.1016/0304-4203(76)90003-7

Coffey, M., Dehairs, F., Collette, O., Luther, G., Church, T., & Jickells, T. (1997). The behaviour of dissolved barium in estuaries. *Estuarine, Coastal and Shelf Science*, *45*(1), 113–121. https://doi.org/10.1006/ecss.1996.0157

Coynel, A., Seyler, P., Etcheber, H., Meybeck, M., & Orange, D. (2005). Spatial and seasonal dynamics of total suspended sediment and organic carbon species in the Congo River. *Global Biogeochemical Cycles*, *19*(4), 1–17. https://doi.org/10.1029/2004GB002335

Dehairs, F., Chesselet, R., & Jedwab, J. (1980). Discrete suspended particles of barite and the barium cycle in the open ocean. *Earth and Planetary Science Letters*, *49*(2), 528–550. https://doi.org/10.1016/0012-821X(80)90094-1

De La Rocha, C. L., Brzezinski, M. A., & DeNiro, M. J. (1997). Fractionation of silicon isotopes by marine diatoms during biogenic silica formation. *Geochimica et Cosmochimica Acta*, *61*(23), 5051–5056. https://doi.org/10.1016/S0016-7037(97)00300-1

DeMaster, D. J., Smith, W. O., Nelson, D. M., & Aller, J. Y. (1996). Biogeochemical processes in Amazon shelf waters: Chemical distributions and uptake rates of silicon, carbon and nitrogen. *Continental Shelf Research*, *16*(5–6), 617–643. https://doi.org/10.1016/0278-4343(95)00048-8

De Souza, G. F., Reynolds, B. C., Johnson, G. C., Bullister, J. L., & Bourdon, B. (2012). Silicon stable isotope distribution traces Southern Ocean export of Si to the eastern South Pacific thermocline. *Biogeosciences*, *9*(11), 4199–4213. https://doi.org/10.5194/bg-9-4199-2012

De Souza, G. F., Reynolds, B. C., Rickli, J., Frank, M., Saito, M. A., Gerringa, L. J. A., & Bourdon, B. (2012). Southern Ocean control of silicon stable isotope distribution in the deep Atlantic Ocean. *Global Biogeochemical Cycles*, *26*(2), 1–13. https://doi.org/10.1029/2011GB004141

Dymond, J., & Collier, R. (1996). Particulate barium fluxes and their relationships to biological productivity. *Deep-Sea Research Part II Topical Studies in Oceanography*, *43*(4–6), 1283–1308. https://doi.org/10.1016/0967-0645(96)00011-2

Dymond, J., Suess, E., & Lyle, M. (1992). Barium in deep-sea sediment: A geochemical proxy for paleoproductivity. *Paleoceanography*, *7*(2), 163–181. https://doi.org/10.1029/92PA00181

Edmond, J. M., Boyle, E. D., Drummond, D., Grant, B., & Mislick, T. (1978). Desorption of barium in the plume of the Zaire (Congo) River. *Netherlands Journal of Sea Research*, *12*(3–4), 324–328. https://doi.org/10.1016/0077-7579(78)90034-0

Eisma, D., & van Bennekom, A. J. (1978). The Zaire river and estuary and the Zaire outflow in the Atlantic Ocean. *Netherlands Journal of Sea Research*, *12*(3–4), 255–272. https://doi.org/10.1016/0077-7579(78)90030-3

Fisher, N. S., Guillard, R. R. L., & Bankston, D. C. (1991). The accumulation of barium by marine phytoplankton grown in culture. *Journal of Marine Research*, *49*(2), 339–354. https://doi.org/10.1357/002224091784995882

Frings, P. J., Clymans, W., Fontorbe, G., De La Rocha, C. L., & Conley, D. J. (2016). The continental Si cycle and its impact on the ocean Si isotope budget. *Chemical Geology*, *425*, 12–36. https://doi.org/10.1016/j.chemgeo.2016.01.020

Fripiat, F., Cavagna, A. J., Dehairs, F., Speich, S., André, L., & Cardinal, D. (2011). Silicon pool dynamics and biogenic silica export in the Southern Ocean inferred from Si-isotopes. *Ocean Science*, *7*(5), 533–547. https://doi.org/10.5194/os-7-533-2011

Gebregiorgis, D., Hathorne, E. C., Sijinkumar, A. V., Nath, B. N., Nürnberg, D., & Frank, M. (2016). South Asian summer monsoon variability during the last ~54 kyrs inferred from surface water salinity and river runoff proxies. *Quaternary Science Reviews*, *138*, 6–15. https://doi.org/10.1016/j.quascirev.2016.02.012

Geilert, S., Grasse, P., Doering, K., Wallmann, K., Ehlert, C., Scholz, F., et al. (2020). Impact of ambient conditions on the Si isotope fractionation in marine pore fluids during early diagenesis. *Biogeosciences*, *17*(7), 1745–1763. https://doi.org/10.5194/bg-17-1745-2020

Georg, R. B., Reynolds, B. C., Frank, M., & Halliday, A. N. (2006). New sample preparation techniques for the determination of Si isotopic compositions using MC-ICPMS. *Chemical Geology*, *235*(1–2), 95–104. https://doi.org/10.1016/j.chemgeo.2006.06.006

Geyman, B. M., Ptacek, J. L., LaVigne, M., & Horner, T. J. (2019). Barium in deep-sea bamboo corals: Phase associations, barium stable isotopes, & prospects for paleoceanography. *Earth and Planetary Science Letters*, *525*, 115751. https://doi.org/10.1016/j.epsl.2019.115751

Grasse, P., Brzezinski, M. A., Cardinal, D., De Souza, G. F., Andersson, P., Closset, I., et al. (2017). GEOTRACES inter-calibration of the stable silicon isotope composition of dissolved silicic acid in seawater. *Journal of Analytical Atomic Spectrometry*, *32*(3), 562–578. https://doi.org/10.1039/c6ja00302h

Guay, C. K. H., McLaughlin, F. A., & Yamamoto-Kawai, M. (2009). Differentiating fluvial components of upper Canada Basin waters on the basis of measurements of dissolved barium combined with other physical and chemical tracers. *Journal of Geophysical Research*, *114*, 1–17. https://doi.org/10.1029/2008jc005099

Hong, Q., Cai, P., Geibert, W., Cao, Z., Stimac, I., Liu, L., & Li, Q. (2018). Benthic fluxes of metals into the Pearl River Estuary based on $^{224}Ra/^{228}Th$ disequilibrium: From alkaline earth (Ba) to redox sensitive elements (U, Mn, Fe). *Geochimica et Cosmochimica Acta*, *237*, 223–239. https://doi.org/10.1016/j.gca.2018.06.036

Hopkins, J., Lucas, M., Dufau, C., Sutton, M., Stum, J., Lauret, O., & Channelliere, C. (2013). Detection and variability of the Congo River plume from satellite derived sea surface temperature, salinity, ocean colour and sea level. *Remote Sensing of Environment*, *139*, 365–385. https://doi.org/10.1016/j.rse.2013.08.015

Horner, T. J., & Crockford, P. W. (2021). *Barium isotopes* (Vol. 7027). Cambridge University Press. https://doi.org/10.1017/9781108865845

Horner, T. J., Kinsley, C. W., & Nielsen, S. G. (2015). Barium-isotopic fractionation in seawater mediated by barite cycling and oceanic circulation. *Earth and Planetary Science Letters*, *430*, 511–522. https://doi.org/10.1016/j.epsl.2015.07.027

Horner, T. J., Little, S. H., Conway, T. M., Farmer, J. R., Hertzberg, J. E., Janssen, D. J., et al. (2021). Bioactive trace metals and their isotopes as paleoproductivity proxies: An assessment using GEOTRACES-era data. *Global Biogeochemical Cycles*, *35*(11), e2020GB006814. https://doi.org/10.1029/2020GB006814

Horner, T. J., Pryer, H. V., Nielsen, S. G., Crockford, P. W., Gauglitz, J. M., Wing, B. A., & Ricketts, R. D. (2017). Pelagic barite precipitation at micromolar ambient sulfate. *Nature Communications*, *8*(1), 1342. https://doi.org/10.1038/s41467-017-01229-5

Hsieh, Y., & Henderson, G. M. (2017). Barium stable isotopes in the global ocean: Tracer of Ba inputs and utilization. *Earth and Planetary Science Letters*, *473*, 269–278. https://doi.org/10.1016/j.epsl.2017.06.024

Huang, W., Cai, W., Powell, R. T., Lohrenz, S. E., Wang, Y., Jiang, L., & Hopkinson, C. S. (2012). The stoichiometry of inorganic carbon and nutrient removal in the Mississippi River plume and adjacent continental shelf. *Biogeosciences*, *9*(7), 2781–2792. https://doi.org/10.5194/bg-9-2781-2012

Hughes, H. J., Sondag, F., Cocquyt, C., Laraque, A., Pandi, A., André, L., & Cardinala, D. (2011). Effect of seasonal biogenic silica variations on dissolved silicon fluxes and isotopic signatures in the Congo River. *Limnology and Oceanography*, *56*(2), 551–561. https://doi.org/10.4319/lo.2011.56.2.0551

Jacquet, S. H. M., Dehairs, F., Cardinal, D., Navez, J., & Delille, B. (2005). Barium distribution across the Southern Ocean frontal system in the Crozet-Kerguelen Basin. *Marine Chemistry*, *95*(3–4), 149–162. https://doi.org/10.1016/j.marchem.2004.09.002

Jeandel, C., Dupre, B., Lebaron, G., Monnin, C., & Minster, J. F. (1996). Longitudinal distributions of dissolved barium, silica and alkalinity in the western and southern Indian Ocean. *Deep-Sea Research Part I Oceanographic Research Papers*, *43*(1), 1–31. https://doi.org/10.1016/0967-0637(95)00098-4

Jeandel, C., & Oelkers, E. H. (2015). The influence of terrigenous particulate material dissolution on ocean chemistry and global element cycles. *Chemical Geology*, *395*, 50–66. https://doi.org/10.1016/j.chemgeo.2014.12.001

Jeandel, C., Tachikawa, K., Bory, A., & Dehairs, F. (2000). Biogenic barium in suspended and trapped material as a tracer of export production in the tropical NE Atlantic (EUMELI sites). *Marine Chemistry*, *71*(1–2), 125–142. https://doi.org/10.1016/S0304-4203(00)00045-1

Joung, D., & Shiller, A. M. (2014). Dissolved barium behavior in Louisiana Shelf waters affected by the Mississippi/Atchafalaya River mixing zone. *Geochimica et Cosmochimica Acta*, *141*, 303–313. https://doi.org/10.1016/j.gca.2014.06.021

Lea, D. W. (1993). Constraints on the alkalinity and circulation of glacial circumpolar deep water from benthic foraminiferal barium. *Global Biogeochemical Cycles*, *7*(3), 695–710. https://doi.org/10.1029/93GB01536

Le Roy, E., Sanial, V., Charette, M. A., Van Beek, P., Lacan, F., Jacquet, H. M. S., et al. (2018). The ^{226}Ra-Ba relationship in the North Atlantic during GEOTRACES-GA01. *Biogeosciences*, *15*(9), 3027–3048. https://doi.org/10.5194/bg-15-3027-2018

Liu, M., & Tanhua, T. (2021). Water masses in the Atlantic Ocean: Characteristics and distributions. *Ocean Science*, *17*(2), 463–486. https://doi.org/10.5194/os-17-463-2021

Martin, J.-M., & Meybeck, M. (1979). Elemental mass-balance of material carried by major world rivers. *Marine Chemistry*, *7*(3), 173–206. https://doi.org/10.1016/0304-4203(79)90039-2

Martinez-Ruiz, F., Paytan, A., Gonzalez-Muñoz, M. T., Jroundi, F., Abad, M. M., Lam, P. J., et al. (2019). Barite formation in the ocean: Origin of amorphous and crystalline precipitates. *Chemical Geology*, *511*, 441–451. https://doi.org/10.1016/j.chemgeo.2018.09.011

Materia, S., Gualdi, S., Navarra, A., & Terray, L. (2012). The effect of Congo River freshwater discharge on Eastern Equatorial Atlantic climate variability. *Climate Dynamics*, *39*(9–10), 2109–2125. https://doi.org/10.1007/s00382-012-1514-x

Matsumoto, K. (2007). Radiocarbon-based circulation age of the world oceans. *Journal of Geophysical Research*, *112*(9), 1–7. https://doi.org/10.1029/2007JC004095

Mayfield, K. K., Eisenhauer, A., Santiago Ramos, D. P., Higgins, J. A., Horner, T. J., Auro, M., et al. (2021). Groundwater discharge impacts marine isotope budgets of Li, Mg, Ca, Sr, and Ba. *Nature Communications*, *12*(1), 1–9. https://doi.org/10.1038/s41467-020-20248-3

McManus, J., Berelson, W. M., Klinkhammer, G. P., Johnson, K. S., Coale, K. H., Anderson, R. F., et al. (1998). Geochemistry of barium in marine sediments: Implications for its use as a paleoproxy. *Geochimica et Cosmochimica Acta*, *62*(21–22), 3453–3473. https://doi.org/10.1016/s0016-7037(98)00248-8

Menzel Barraqueta, J.-L. (2018). The biogeochemical cycle of dissolved aluminium in the Atlantic Ocean. Retrieved from https://macau.uni-kiel.de/receive/diss_mods_00023074

Milliman, J. D., & Farnsworth, K. L. (2011). *River discharge to the coastal ocean*. Cambridge University Press. https://doi.org/10.1017/CBO9780511781247

Moore, W. S. (1997). High fluxes of radium and barium from the mouth of the Ganges-Brahmaputra River during low river discharge suggest a large groundwater source. *Earth and Planetary Science Letters*, *150*(1–2), 141–150. https://doi.org/10.1016/s0012-821x(97)00083-6

Ng, H. C., Cassarino, L., Pickering, R. A., Woodward, E. M. S., Hammond, S. J., & Hendry, K. R. (2020). Sediment efflux of silicon on the Greenland margin and implications for the marine silicon cycle. *Earth and Planetary Science Letters*, *529*, 115877. https://doi.org/10.1016/j.epsl.2019.115877

Nittrouer, C. A., & DeMaster, D. J. (1996). The Amazon shelf setting: Tropical, energetic, and influenced by a large river. *Continental Shelf Research*, *16*(5–6), 553–573. https://doi.org/10.1016/0278-4343(95)00069-0

Nozaki, Y., Yamamoto, Y., Manaka, T., Amakawa, H., & Snidvongs, A. (2001). Dissolved barium and radium isotopes in the Chao Phraya River estuarine mixing zone in Thailand. *Continental Shelf Research*, *21*(13–14), 1435–1448. https://doi.org/10.1016/S0278-4343(01)00023-1

Pastor, L., Toffin, L., Decker, C., Olu, K., Cathalot, C., Lesongeur, F., et al. (2017). Early diagenesis in the sediments of the Congo deep-sea fan dominated by massive terrigenous deposits: Part III – Sulfate- and methane- based microbial processes. *Deep-Sea Research Part II Topical Studies in Oceanography*, *142*, 139–150. https://doi.org/10.1016/j.dsr2.2017.03.011

Percuoco, V. P., Kalnejais, L. H., & Officer, L. V. (2015). Nutrient release from the sediments of the Great Bay Estuary, N.H. USA. *Estuarine, Coastal and Shelf Science*, *161*, 76–87. https://doi.org/10.1016/j.ecss.2015.04.006

Peterson, R. G., & Stramma, L. (1991). Upper-level circulation in the South Atlantic Ocean. *Progress in Oceanography*, *26*(1), 1–73. https://doi.org/10.1016/0079-6611(91)90006-8

Pozzato, L., Cathalot, C., Berrached, C., Toussaint, F., Stetten, E., Caprais, J. C., et al. (2017). Early diagenesis in the Congo deep-sea fan sediments dominated by massive terrigenous deposits: Part I – Oxygen consumption and organic carbon mineralization using a micro-electrode approach. *Deep-Sea Research Part II Topical Studies in Oceanography*, *142*, 125–138. https://doi.org/10.1016/j.dsr2.2017.05.010

Rabouille, C., Dennielou, B., Baudin, F., Raimonet, M., Droz, L., Khripounoff, A., et al. (2019). Carbon and silica megasink in deep-sea sediments of the Congo terminal lobes. *Quaternary Science Reviews*, *222*, 105854. https://doi.org/10.1016/j.quascirev.2019.07.036

Ragueneau, O., Gallinari, M., Corrin, L., Grandel, S., Hall, P., Hauvespre, A., et al. (2001). The benthic silica cycle in the Northeast Atlantic: Annual mass balance, seasonality, and importance of non-steady-state processes for the early diagenesis of biogenic opal in deep-sea sediments. *Progress in Oceanography*, *50*(1–4), 171–200. https://doi.org/10.1016/S0079-6611(01)00053-2

Ragueneau, O., Regaudie-de-Gioux, A., Moriceau, B., Gallinari, M., Vangriesheim, A., Baurand, F., & Khripounoff, A. (2009). A benthic Si mass balance on the Congo margin: Origin of the 4000 m DSi anomaly and implications for the transfer of Si from land to ocean. *Deep-Sea Research Part II Topical Studies in Oceanography*, *56*(23), 2197–2207. https://doi.org/10.1016/j.dsr2.2009.04.003

Rahlf, P., Hathorne, E., Laukert, G., Gutjahr, M., Weldeab, S., & Frank, M. (2020). Tracing water mass mixing and continental inputs in the southeastern Atlantic Ocean with dissolved neodymium isotopes. *Earth and Planetary Science Letters*, *530*, 115944. https://doi.org/10.1016/j.epsl.2019.115944

Rahlf, P., Laukert, G., Hathorne, E. C., Vieira, L. H., & Frank, M. (2021). Dissolved neodymium and hafnium isotopes and rare earth elements in the Congo River Plume: Tracing and quantifying continental inputs into the southeast Atlantic. *Geochimica et Cosmochimica Acta*, *294*, 192–214. https://doi.org/10.1016/j.gca.2020.11.017

Rahman, S., Shiller, A. M., Anderson, R. F., Charette, M. A., Hayes, C. T., Gilbert, M., et al. (2022). Dissolved and particulate barium distributions along the US GEOTRACES North Atlantic and East Pacific Zonal transects (GA03 and GP16): Global implications for the marine barium cycle. *Global Biogeochemical Cycles*, *36*(6), 1–78. https://doi.org/10.1029/2022gb007330

Rahman, S., Tamborski, J. J., Charette, M. A., & Cochran, J. K. (2019). Dissolved silica in the subterranean estuary and the impact of submarine groundwater discharge on the global marine silica budget. *Marine Chemistry*, *208*, 29–42. https://doi.org/10.1016/j.marchem.2018.11.006

Raimonet, M., Ragueneau, O., Andrieux-Loyer, F., Philippon, X., Kerouel, R., Le Goff, M., & Mémery, L. (2013). Spatio-temporal variability in benthic silica cycling in two macrotidal estuaries: Causes and consequences for local to global studies. *Estuarine, Coastal and Shelf Science*, *119*, 31–43. https://doi.org/10.1016/j.ecss.2012.12.008

Raimonet, M., Ragueneau, O., Jacques, V., Corvaisier, R., Moriceau, B., Khripounoff, A., et al. (2015). Rapid transport and high accumulation of amorphous silica in the Congo deep-sea fan: A preliminary budget. *Journal of Marine Systems*, *141*, 71–79. https://doi.org/10.1016/j.jmarsys.2014.07.010

Reynolds, B. C., Aggarwal, J., André, L., Baxter, D., Beucher, C., Brzezinski, M. A., et al. (2007). An inter-laboratory comparison of Si isotope reference materials. *Journal of Analytical Atomic Spectrometry*, *22*(5), 561–568. https://doi.org/10.1039/b616755a

Reynolds, B. C., Frank, M., & Halliday, A. N. (2006). Silicon isotope fractionation during nutrient utilization in the North Pacific. *Earth and Planetary Science Letters*, *244*(1–2), 431–443. https://doi.org/10.1016/j.epsl.2006.02.002

Samanta, S., & Dalai, T. K. (2016). Dissolved and particulate Barium in the Ganga (Hooghly) River estuary, India: Solute-particle interactions and the enhanced dissolved flux to the oceans. *Geochimica et Cosmochimica Acta*, *195*, 1–28. https://doi.org/10.1016/j.gca.2016.09.005

Savoye, B., Babonneau, N., Dennielou, B., & Bez, M. (2009). Geological overview of the Angola-Congo margin, the Congo deep-sea fan and its submarine valleys. *Deep-Sea Research Part II Topical Studies in Oceanography*, *56*(23), 2169–2182. https://doi.org/10.1016/j.dsr2.2009.04.001

Sayles, F. L., Deuser, W. G., Goudreau, J. E., Dickinson, W. H., Jickells, T. D., & King, P. (1996). The benthic cycle of biogenic opal at the Bermuda Atlantic Time Series site. *Deep-Sea Research Part I Oceanographic Research Papers*, *43*(4), 383–409. https://doi.org/10.1016/0967-0637(96)00027-1

Schlitzer, R. (2021). Ocean Data View. Retrieved from https://odv.awi.de

Scholz, F., Cheng, J., Zhang, Z., Vosteen, P., Siebert, C., & Frank, M. (2023). Benthic-pelagic coupling and isotopic fractionation of barium in Kiel Bight, SW Baltic Sea. *Frontiers in Marine Science*, *10*, 1–14. https://doi.org/10.3389/fmars.2023.1101095

Spencer, R. G. M., Stubbins, A., & Gaillardet, J. (2013). Geochemistry of the Congo River, estuary, and plume. *Biogeochemical Dynamics at Major River-Coastal Interfaces*, 554–583. https://doi.org/10.1017/cbo9781139136853.027

Sternberg, E., Tang, D., Ho, T. Y., Jeandel, C., & Morel, F. M. M. (2005). Barium uptake and adsorption in diatoms. *Geochimica et Cosmochimica Acta*, *69*(11), 2745–2752. https://doi.org/10.1016/j.gca.2004.11.026

Sutton, J. N., André, L., Cardinal, D., Conley, D. J., De Souza, G. F., Dean, J., et al. (2018). A review of the stable isotope bio-geochemistry of the global silicon cycle and its associated trace elements. *Frontiers in Earth Science*, *5*, 112. https://doi.org/10.3389/feart.2017.00112

Sutton, J. N., Varela, D. E., Brzezinski, M. A., & Beucher, C. P. (2013). Species-dependent silicon isotope fractionation by marine diatoms. *Geochimica et Cosmochimica Acta*, *104*, 300–309. https://doi.org/10.1016/j.gca.2012.10.057

Taillefert, M., Beckler, J. S., Cathalot, C., Michalopoulos, P., Corvaisier, R., Kiriazis, N., et al. (2017). Early diagenesis in the sediments of the Congo deep-sea fan dominated by massive terrigenous deposits: Part II – Iron–sulfur coupling. *Deep-Sea Research Part II Topical Studies in Oceanography*, *142*, 151–166. https://doi.org/10.1016/j.dsr2.2017.06.009

Tallberg, P., Heiskanen, A. S., Niemistö, J., Hall, P. O. J., & Lehtoranta, J. (2017). Are benthic fluxes important for the availability of Si in the Gulf of Finland? *Journal of Marine Systems*, *171*, 89–100. https://doi.org/10.1016/j.jmarsys.2017.01.010

Talling, P. J., Baker, M. L., Pope, E. L., Ruffell, S. C., Jacinto, R. S., Heijnen, M. S., et al. (2022). Longest sediment flows yet measured show how major rivers connect efficiently to deep sea. *Nature Communications*, *13*(1), 1–15. https://doi.org/10.1038/s41467-022-31689-3

Tréguer, P. J., Sutton, J. N., Brzezinski, M., Charette, M. A., Devries, T., Dutkiewicz, S., et al. (2021). Reviews and syntheses: The biogeochemical cycle of silicon in the modern ocean. *Biogeosciences*, *18*(4), 1269–1289. https://doi.org/10.5194/bg-18-1269-2021

Vallaeys, V., Lambrechts, J., Delandmeter, P., Pätsch, J., Spitzy, A., Hanert, E., & Deleersnijder, E. (2021). Understanding the circulation in the deep, micro-tidal and strongly stratified Congo River estuary. *Ocean Modelling*, *167*, 101890. https://doi.org/10.1016/j.ocemod.2021.101890

Vangriesheim, A., Pierre, C., Aminot, A., Metzl, N., Baurand, F., & Caprais, J. C. (2009). The influence of Congo River discharges in the surface and deep layers of the Gulf of Guinea. *Deep-Sea Research Part II Topical Studies in Oceanography*, *56*(23), 2183–2196. https://doi.org/10.1016/j.dsr2.2009.04.002

Vieira, L. H. (2019). *Radium isotopes as tracers of element cycling at ocean boundaries*. Retrieved from https://macau.uni-kiel.de/receive/diss_mods_00025629

Vieira, L. H., Krisch, S., Hopwood, M. J., Beck, A. J., Scholten, J., Liebetrau, V., & Achterberg, E. P. (2020). Unprecedented Fe delivery from the Congo River margin to the South Atlantic Gyre. *Nature Communications*, *11*(1), 1–8. https://doi.org/10.1038/s41467-019-14255-2

Ward, J. P. J., Hendry, K. R., Arndt, S., Faust, J. C., Freitas, F. S., Henley, S. F., et al. (2022). Stable silicon isotopes uncover a mineralogical control on the benthic silicon cycle in the Arctic Barents Sea. *Geochimica et Cosmochimica Acta*, *329*, 206–230. https://doi.org/10.1016/j.gca.2022.05.005

Weldeab, S., Lea, D. W., Schneider, R. R., & Andersen, N. (2007). Centennial scale climate instabilities in a wet early Holocene West African monsoon. *Geophysical Research Letters*, *34*(24), 1–6. https://doi.org/10.1029/2007GL031898

Whitmore, L. M., Shiller, A. M., Horner, T. J., Xiang, Y., Auro, M. E., Bauch, D., et al. (2022). Strong margin influence on the Arctic Ocean barium cycle revealed by Pan-Arctic synthesis. *Journal of Geophysical Research: Oceans*, *127*(4), 1–28. https://doi.org/10.1029/2021JC017417

Yu, Y., Siebert, C., Fietzke, J., Goepfert, T., Hathorne, E., Cao, Z., & Frank, M. (2020). The impact of MC-ICP-MS plasma conditions on the accuracy and precision of stable isotope measurements evaluated for barium isotopes. *Chemical Geology*, *549*, 119697. https://doi.org/10.1016/j.chemgeo.2020.119697

Yu, Y., Xie, R. C., Gutjahr, M., Laukert, G., Cao, Z., Hathorne, E., et al. (2022). High latitude controls on dissolved barium isotope distributions in the global ocean. *Geochemical Perspectives Letters*, *24*, 22–26. https://doi.org/10.7185/geochemlet.2242

Zhang, Z., Cao, Z., Grasse, P., Dai, M., Gao, L., Kuhnert, H., et al. (2020). Dissolved silicon isotope dynamics in large river estuaries. *Geochimica et Cosmochimica Acta*, *273*, 367–382. https://doi.org/10.1016/j.gca.2020.01.028

Zhang, Z., Sun, X., Dai, M., Cao, Z., Fontorbe, G., & Conley, D. J. (2020). Impact of human disturbance on the biogeochemical silicon cycle in a coastal sea revealed by silicon isotopes. *Limnology and Oceanography*, *65*(3), 515–528. https://doi.org/10.1002/lno.11320

Zheng, X. Y., Plancherel, Y., Saito, M. A., Scott, P. M., & Henderson, G. M. (2016). Rare earth elements (REEs) in the tropical South Atlantic and quantitative deconvolution of their non-conservative behavior. *Geochimica et Cosmochimica Acta*, *177*, 217–237. https://doi.org/10.1016/j.gca.2016.01.018

References From the Supporting Information

Dai, A., Qian, T., Trenberth, K. E., & Milliman, J. D. (2009). Changes in continental freshwater discharge from 1948 to 2004. *Journal of Climate*, *22*(10), 2773–2792. https://doi.org/10.1175/2008JCLI2592.1

Mohrholz, V., Schmidt, M., & Lutjeharms, J. R. E. (2001). The hydrography and dynamics of the Angola-Benguela Frontal Zone and environment in April 1999. *South African Journal of Science*, *97*, 199–208.

Siebert, C., Nägler, T. F., & Kramers, J. D. (2001). Determination of molybdenum isotope fractionation by double-spike multicollector inductively coupled plasma mass spectrometry. *Geochemistry, Geophysics, Geosystems*, *2*(7), 1032. https://doi.org/10.1029/2000GC000124

Tchipalanga, P., Dengler, M., Brandt, P., Kopte, R., Macuéria, M., Coelho, P., et al. (2018). Eastern boundary circulation and hydrography off Angola building Angolan oceanographic capacities. *Bulletin of the American Meteorological Society*, *99*(8), 1589–1605. https://doi.org/10.1175/BAMS-D-17-0197.1

Young, E. D., Galy, A., & Nagahara, H. (2002). Kinetic and equilibrium mass-dependent isotope fractionation laws in nature and their geochemical and cosmochemical significance. *Geochimica et Cosmochimica Acta*, *66*(6), 1095–1104. https://doi.org/10.1016/S0016-7037(01)00832-8